

1  
2  
3 1 **Dynamics of former ice lobes of the southernmost Patagonian Ice Sheet based on a**  
4  
5 2 **glacial landsystems approach**  
6

---

7  
8 3 Christopher M. Darvill\*<sup>1,†</sup>, Chris R. Stokes<sup>1</sup>, Michael J. Bentley<sup>1</sup>, David, J. A. Evans<sup>1</sup> & Harold  
9 4 Lovell<sup>2</sup>

10  
11  
12  
13 5 \*E-mail: [christopher.darvill@unbc.ca](mailto:christopher.darvill@unbc.ca)

14  
15  
16 6 <sup>1</sup> Department of Geography, Durham University, South Road, Durham, DH1 3LE, UK.

17  
18 7 <sup>2</sup> Department of Geography, University of Portsmouth, Portsmouth, UK.

19  
20  
21 8 † Present address: Geography Program and Natural Resources and Environmental Studies Institute,  
22 9 University of Northern British Columbia, 3333 University Way, Prince George, BC, V2N 4Z9, Canada.

23  
24  
25 10  
26  
27

---

1  
2  
3 11 **Abstract**  
4  
5

6 12 Reconstructions of former ice masses from glacial geomorphology help constrain the nature  
7  
8 13 and timing of glaciation in relation to climatic forcing. This paper presents a new  
9  
10 14 reconstruction of the glacial history of five ice lobes in southernmost South America: the  
11  
12 15 Bahía Inútil – San Sebastián, Magellan, Otway, Skyring, and Río Gallegos ice lobes. We use  
13  
14 16 previous geomorphological mapping of glacial landforms to reconstruct former glacial limits  
15  
16 17 and proglacial lakes, demarcate flow-sets from the distribution of glacial lineations, and  
17  
18 18 evaluate glacial landsystem signatures and their palaeoglaciological implications. Evidence  
19  
20 19 suggests that the ice lobes predominantly reflect active temperate glacial landsystems,  
21  
22 20 which may have switched to polythermal systems when periods of cold-based ice developed  
23  
24 21 ephemerally. This complex landsystem signature implies that the ice lobes were sensitive to  
25  
26 22 regional climate variability, with active re-advances during overall retreat of the ice margins.  
27  
28 23 There is also evidence for periods of fast ice flow and possible surge-like activity in the  
29  
30 24 region, followed by the rapid retreat or even collapse of some of the ice lobes in association  
31  
32 25 with proglacial lakes. Constraining our new reconstruction with published chronological  
33  
34 26 information suggests that at least some of the ice lobes advanced prior to the global Last  
35  
36 27 Glacial Maximum (gLGM: *ca.* 26.5-19 ka) during the last glacial cycle. Our new  
37  
38 28 reconstruction demonstrates a more complex picture of ice dynamics than has previously  
39  
40 29 been portrayed, and one in which the advance and retreat of the ice lobes was likely to have  
41  
42 30 been primarily driven by changes in climate. As such, ice advances prior to the gLGM in the  
43  
44 31 southernmost part of the Patagonian Ice Sheet are likely to be indicative of a wider climatic  
45  
46 32 forcing at this time.  
47  
48  
49  
50  
51  
52  
53  
54  
55  
56  
57  
58  
59  
60

## 1 Introduction

Well-preserved glacial geomorphology relating to the former Patagonian Ice Sheet provides a record of the fluctuations of its margins throughout the Quaternary (Clapperton, 1993; Glasser & Jansson, 2008; Glasser et al., 2008). This record can also be used to reconstruct ice-sheet dynamics (Glasser & Jansson, 2005; Glasser et al., 2005; Lovell et al., 2012) and may be supplemented with chronological information to constrain how the ice sheet changed over time as a result of climatic forcing (e.g. McCulloch et al., 2005b; Douglass et al., 2006; Kaplan et al., 2008a, 2008b; Hein et al., 2010). For example, the southernmost part of the ice sheet was heavily influenced by changes in temperature and precipitation linked to the atmospheric Southern Westerly Winds and oceanic frontal positions (Lamy et al., 2007; Kaplan et al., 2008a; Kilian & Lamy, 2012). Climate reconstructions prior to the Holocene are uncertain, but temperatures at the global Last Glacial Maximum (gLGM: ca. 26.5-19 ka, Clark et al., 2009) may have been as much as 7-8°C lower than present (Benn & Clapperton, 2000a; Caniupán et al., 2011). Consequently, reconstruction of the southernmost ice lobes can help to establish likely changes in these climatic systems over time, but this process requires a robust understanding of the glacial history and ice dynamics (Sugden et al., 2005; Kilian & Lamy, 2012).

Previous studies of the southernmost ice lobes of the Patagonian Ice Sheet have tended to focus on dating glacial limits, with a particular emphasis on constraining the local Last Glacial Maximum in relation to the gLGM and younger glacial limits. However, there has been a lack of consistent, detailed mapping across the region (Darvill et al., 2014), and there remains uncertainty about the timing and nature of pre-gLGM glacial advances (Kaplan et al., 2007). Indeed, it has been shown that glacial limits of the Bahía Inútil – San Sebastián (BI-SSb) ice lobe that were previously thought to be pre-last glacial cycle were actually deposited more recently (Darvill et al., 2015b). This suggests that significant glacier advances during Marine Isotope Stage (MIS) 3 (and possibly MIS 4) are represented in the area, perhaps linked to wider glacial activity in the southern mid-latitudes at this time

1  
2  
3 60 (Putnam et al., 2013; Kelley et al., 2014; Darvill et al., 2015b; Doughty et al., 2015; Schaefer  
4  
5 61 et al., 2015; Eaves et al., 2016). In this paper, we use a previously published map of the  
6  
7 62 region, largely based on relatively high-resolution satellite imagery (~30 m resolution; Darvill  
8  
9 63 et al., 2014), and apply glacial inversion methods to produce a new palaeoglaciological  
10  
11 64 reconstruction of the dynamics of the ice sheet that is further constrained through analysis of  
12  
13 65 published chronological data.  
14  
15

16 66

## 17 18 19 67 **2 Study area**

20  
21  
22 68 The study area lies between 51-55°S and 68-73°W, and encompasses the area occupied by  
23  
24 69 five former piedmont ice lobes of the Patagonian Ice Sheet (Figure 1). From south to north,  
25  
26 70 these are the Bahía Inútil – San Sebastián (BI-SSb), Magellan, Otway, Skyring and Río  
27  
28 71 Gallegos lobes. The topography of the area changes dramatically from southwest to  
29  
30 72 northeast, with the southern Andes (dominated by the Cordillera Darwin) marking the  
31  
32 73 southern and western boundaries and casting a strong rain shadow over the low, flat  
33  
34 74 pampas and coastal areas to the north and east (Coronato et al., 2008). The locations of the  
35  
36 75 former ice lobes are marked by prominent straits and sounds, which were established by  
37  
38 76 one or more major glacial events during the Quaternary (Rabassa, 2008; Kaplan et al.,  
39  
40 77 2009). Glacial geomorphology relating to the former ice lobes was first described in detail by  
41  
42 78 Caldenius (1932) and has since been updated, and sometimes reinterpreted, by numerous  
43  
44 79 workers (Clapperton et al., 1995; Rabassa et al., 2000; Benn & Clapperton, 2000b, 2000a;  
45  
46 80 Meglioli, 1992; Bentley et al., 2005; McCulloch et al., 2005b; Lovell et al., 2011, 2012; Darvill  
47  
48 81 et al., 2014, 2015a).

49  
50  
51 82 Meglioli (1992) used weathering indices to establish an age model for the region, whereby  
52  
53 83 nested moraine limits were deposited during successive glacial episodes from MIS 12 to 2  
54  
55 84 (Coronato et al., 2004). Subsequently, a range of dating techniques have been used to  
56  
57 85 constrain the ages of some moraine limits deposited during or after the gLGM (Rutter et al.,  
58  
59  
60

1  
2  
3 86 1989; Porter, 1990; Meglioli, 1992; Clapperton et al., 1995; McCulloch et al., 2005b; Sagredo  
4  
5 87 et al., 2011; Blomdin et al., 2012; Hall et al., 2013). Age constraints prior to the gLGM are  
6  
7 88 limited (Kaplan et al., 2007; Evenson et al., 2009; Darvill et al., 2015a, 2015b), although  
8  
9 89  $^{40}\text{Ar}/^{39}\text{Ar}$  dates suggest that the outermost limits of the Río Gallegos, Skyring, Otway and  
10  
11 90 Magellan lobes date to 1070-450 ka (Meglioli, 1992; Singer et al., 2004). By contrast, Darvill  
12  
13 91 et al. (2015b) recently demonstrated that one of two outer limits of the BI-SSb lobe was  
14  
15 92 deposited much more recently, at ca. 30 ka. Beyond this, the Magellan and Río Gallegos  
16  
17 93 lobes have only a few scattered cosmogenic nuclide exposure ages (Kaplan et al., 2007;  
18  
19 94 Evenson et al., 2009; Sagredo et al., 2011) and the Skyring and Otway lobes have no age  
20  
21 95 controls prior to around 15 ka (Kilian et al., 2007, 2013).

22  
23  
24 96 Relatively little attention has been given to the nature of ice dynamics recorded by the glacial  
25  
26 97 geomorphology, with the exception of localised studies on the gLGM or post-gLGM limits.  
27  
28 98 Previous work has highlighted factors affecting ice-lobe dynamics and rates of advance and  
29  
30 99 retreat, such as the influence of pro-glacial lakes (Porter et al., 1992; Lovell et al., 2012),  
31  
32 100 subglacial thermal regime (Benn & Clapperton, 2000b, 2000a; Bentley et al., 2005) and  
33  
34 101 evidence for rapid ice flow over a soft-sediment bed (Clapperton et al., 1995; Lovell et al.,  
35  
36 102 2012). As such, there is a need for a regional glacial history that incorporates  
37  
38 103 geomorphological evidence for ice dynamics and reassesses previously published  
39  
40 104 chronological data.

41  
42  
43 105

### 44 45 46 106 **3 Methods**

#### 47 48 49 107 **3.1 Geomorphological mapping**

50  
51  
52 108 This paper uses a previously-published glacial geomorphological map of the region (Darvill  
53  
54 109 et al., 2014) to build a new palaeoglaciological reconstruction. Glacial landforms were  
55  
56 110 mapped from Landsat and ASTER satellite images, aerial photographs, Google Earth  
57  
58 111 imagery, and SRTM digital elevation data, and much of the area was also cross-checked in

1  
2  
3 112 the field, with an emphasis on verifying mapped landforms and identifying cross-cutting  
4  
5 113 relationships of features (Darvill et al., 2014).  
6  
7  
8 114

9  
10  
11 115 **3.2 *Glacial flow-sets, ice margins and landsystems***

12  
13 116 Glacial landforms can yield information on the extent of former ice advances and ice sheet  
14  
15 117 dynamics using glacial inversion methods (Kleman et al., 2006). Glacial lineation flow-sets  
16  
17 118 reveal coherent patterns of former ice flow trajectories and a landsystem approach links  
18  
19 119 assemblages of glacial geomorphological features to particular styles of glaciation (Evans,  
20  
21 120 2003a), many of which have modern analogues that aid the interpretation of former glacial  
22  
23 121 and climatic conditions. Following Clark (1999), glacial lineations were grouped into flow-sets  
24  
25 122 according to parallel concordance, close proximity and similar morphometry, as well as  
26  
27 123 relationship to ice marginal features such as moraines and meltwater channels. By mapping  
28  
29 124 glacial landforms systematically and comprehensively, we were able to both reconstruct  
30  
31 125 glacial limits and assess landsystem types and their palaeoglaciological implications based  
32  
33 126 on landform suites.  
34  
35

36 127

37  
38  
39 128 **3.3 *Proglacial lake reconstruction***

40  
41 129 The reconstruction of former proglacial lakes can yield information on the relative position of  
42  
43 130 ice lobes and their dynamics. Following Stokes & Clark (2004) and Lovell et al. (2012), we  
44  
45 131 modelled proglacial lake formation using a Digital Elevation Model (DEM), constructed from  
46  
47 132 ca. 90 m resolution SRTM data for areas of land, and ca. 900 m resolution ETOPO data for  
48  
49 133 submarine areas that may have been previously exposed. The DEM was filled in 10 m  
50  
51 134 increments to examine where lakes developed and over-spilled in relation to former  
52  
53 135 shorelines and ice margins. The DEM data is sufficient for a regional-scale assessment of  
54  
55 136 where lakes were likely to have developed (*cf.* Lovell et al., 2012), but the coarser resolution  
56  
57 137 of the ETOPO data means that over-spill channels beneath present sea-level may have  
58  
59  
60

1  
2  
3 138 been missed, and a lack of bathymetric data for present-day lakes means that their exact  
4  
5 139 depths are unknown. Additionally, the DEM provides present-day land elevation and not that  
6  
7 140 during glaciation, when the mass of the Patagonian Ice Sheet would have depressed the  
8  
9 141 mountain range. This should be corrected for Glacio-Isostatic Adjustment (GIA), but the  
10  
11 142 resolution of global model output, such as ICE-5G (Peltier, 2004), is too coarse to be of use  
12  
13 143 for this purpose. Consequently, we reconstructed palaeolakes based on a contemporary  
14  
15 144 DEM, but with the caution that they are likely minimum estimates of lake depth because the  
16  
17 145 regional pattern of ice loading would have been to overdeepen slopes towards the west. The  
18  
19 146 presence of lakes predicted by the DEM analysis was cross-checked and, although the field  
20  
21 147 evidence is inherently fragmentary, we did not identify any obvious conflict between  
22  
23 148 predicted lake levels and the presence of raised shorelines in the glacial geomorphological  
24  
25 149 mapping.  
26  
27

28 150

## 31 151 **4 Glacial Landform Assemblages**

32  
33  
34 152 This section summarises the nature of the glacial landform assemblages in the study area.  
35  
36 153 The results are in the form of a map published in Darvill et al. (2014) and we now describe  
37  
38 154 and interpret the landform assemblages before discussing their palaeoglaciological  
39  
40 155 significance in section 5.  
41  
42

### 43 156 **4.1 Ice-marginal landforms**

#### 44 157 **4.1.1 Moraine ridges**

45  
46  
47  
48 158 The clearest moraine ridges in the study area are those of the Skyring and Otway lobes,  
49  
50 159 where numerous arcuate ridges are nested around the main depressions (Figure 2), marking  
51  
52 160 the point at which the lobes were flowing up the adverse slopes of overdeepenings onto  
53  
54 161 higher relief areas (Barr & Lovell, 2014). Similar moraines are found on the northern side of  
55  
56 162 the Magellan lobe, particularly across Primera Angostura (Figure 2), within ca. 10 km of  
57  
58  
59  
60

1  
2  
3 163 Bahía Inútil in the BI-SSb lobe (Figure 3), and in the Río Gallegos lobe depression. Smaller,  
4  
5 164 less distinctive ridges aligned perpendicular to former ice flow are often draped over other  
6  
7 165 glacial features within the central Magellan and BI-SSb lobes, such as on Punta Gente,  
8  
9 166 where ridges are draped over drumlinised terrain north of Porvenir (Bentley et al., 2005;  
10  
11 167 Figure 4). Likewise, in the centre of the BI-SSb depression, ridges can be seen draped over  
12  
13 168 both lineations and subdued moraine topography (Figure 3).

14  
15  
16 169 The ridges include terminal moraines (sharp-crested, arcuate ridges around the main  
17  
18 170 depressions) and recessional moraines or recessional push moraines (smaller, less  
19  
20 171 distinctive ridges perpendicular to ice flow and draping other features), although it is difficult  
21  
22 172 to distinguish their form based on morphology alone. Two exceptions are where we have  
23  
24 173 supplementary sedimentological evidence to support the landform data. A section through a  
25  
26 174 moraine in the BI-SSb lobe shows silts and sands that have been strongly faulted and folded  
27  
28 175 (Figure 5). Similarly, sediments within one of the moraine ridges in the Otway lobe show  
29  
30 176 faulted sands and gravels (Figure 6). The deformation of moraine sediments in this way is  
31  
32 177 indicative of proglacial glaciotectonism (Rotnicki, 1976; Aber, 1985; Aber et al., 1989; van  
33  
34 178 der Wateren, 1995), and we interpret the deformation to represent thrusting and folding  
35  
36 179 during active re-advances of the ice lobes (Oldale & O'Hara, 1984; Harris et al., 1997;  
37  
38 180 Williams et al., 2001; Evans & Twigg, 2002; Phillips et al., 2002, 2008b, 2008a), at least in  
39  
40 181 these two locations. The BI-SSb moraine contains deformed lacustrine silts, indicating that  
41  
42 182 the timing and extent of retreat and re-advance was sufficient to allow a proglacial lake to  
43  
44 183 accumulate. Our interpretation suggests that some of the moraine ridges may be part of  
45  
46 184 composite thrust complexes, similar to those reported around the Strait of Magellan  
47  
48 185 (Clapperton et al., 1995; Benn & Clapperton, 2000a, 2000b).

50  
51 186  
52  
53  
54  
55  
56  
57  
58  
59  
60

## 187 4.1.2 Hummocky terrain

188 Hummocky terrain is abundant within the BI-SSb lobe (Figure 3), but is also found in  
189 association with the Magellan lobe (Figure 4). It consists of semi-rounded hills and hollows at  
190 both smaller (e.g.  $\leq 5$  m relief) and larger ( $> 5$  m relief) scales, with the smaller hummocky  
191 terrain forming arcuate bands running parallel to moraine ridges. The hummocks are  
192 predominantly irregular and chaotic and were classified as 'irregular hummocky terrain'  
193 (smaller hummocky terrain) and 'kettle-kame topography' (larger hummocky terrain) by  
194 Darvill et al. (2014).

195 Hummocky terrain is typically associated with deposition of supraglacial debris (Boulton,  
196 1972; Benn, 1992; Kjaer & Kruger, 2001; Johnson & Clayton, 2003; Schomacker, 2008),  
197 although the transport pathway of debris resulting in this terrain is often conjectural (Evans,  
198 2009, and references therein). We infer that the disorganised nature of the landform is  
199 indicative of periods of ice stagnation and down-wasting during overall recession of the ice  
200 lobes, leaving behind buried ice and resulting in topographic inversion of the terrain (Clayton,  
201 1964; Boulton, 1972; Etzelmüller et al., 1996; Kjaer & Kruger, 2001; Schomacker, 2008).  
202 More specifically, the organisation of hummocky terrain in arcuate bands has been  
203 interpreted as the product of incremental stagnation (*sensu* Eyles, 1979; Bennett & Evans,  
204 2012) in other lowland settings (e.g. Attig et al., 1989; Ham & Attig, 1996; Clayton et al.,  
205 2001; Dyke & Evans, 2003; Evans et al., 2014), a process-form regime that could also apply  
206 to the settings described here if the glacier lobes were episodically carrying large englacial  
207 and supraglacial debris loads.

208 Bands of larger hummocky terrain mark the Primera Angostura and Segunda Angostura  
209 limits of the Magellan lobe (Meglioli, 1992; Benn & Clapperton, 2000a, 2000b; Rabassa,  
210 2008; Figure 2), but are seen most clearly as a double band on both the north and south  
211 sides of the BI-SSb depression (Figures 1, 3, 7). This landform was described as 'kettle and  
212 kame topography' by (Darvill et al., 2014), but the nomenclature is problematic given that  
213 there is no sedimentary evidence for kames and similar features in North America have an

1  
2  
3 214 ambiguous origin (*sensu* Evans, 2009). Rather, we tentatively group the landform with  
4  
5 215 hummocky terrain and suggest that further sedimentary work is required to establish the full  
6  
7 216 nature of this geomorphology. The topography consists of chaotic hills surrounding rounded  
8  
9 217 hollows, and delimited by broad outwash plains. Darvill et al. (2015a) mapped a series of  
10  
11 218 erratic boulder trains along the southern edge of the BI-SSb lobe, two of which drape over  
12  
13 219 the larger hummocky terrain. A deep section through the inner band of the BI-SSb lobe (the  
14  
15 220 San Sebastián drift) shows two basal diamict units separated by outwash sands and gravels  
16  
17 221 (Figure 7). This implies that the ice lobe advanced to form the outer (Río Cullen) band first  
18  
19 222 before retreating into the BI-SSb depression and subsequently re-advancing.  
20  
21

22 223

#### 24 224 4.1.3 Geometrical ridges

25  
26  
27 225 A large swath of strikingly linear cross-cutting ridges occurs north of Laguna Larga in the  
28  
29 226 central BI-SSb depression. These are regularly-orientated geometrical ridge networks  
30  
31 227 (*sensu* Bennett et al., 1996), described as 'regular hummocky terrain' by Darvill et al. (2014;  
32  
33 228 Figures 3B and 8). They comprise discontinuous, cross-cutting, conjugate paired ridges,  
34  
35 229 generally orientated perpendicular to former ice flow. Although long-regarded as the  
36  
37 230 remnants of crevasse-squeeze ridges, and also diagnostic of glacier surges in a  
38  
39 231 landsystems sense (Raedecke, 1978; Sharp, 1985; Bennett et al., 1996), such landforms  
40  
41 232 have since also been related to: a) active temperate glacier lobes, where they occur in  
42  
43 233 narrow concentric arcs in association with sawtooth style push moraines (Evans & Twigg,  
44  
45 234 2002; Evans et al., 2015); and b) ice stream shutdown, where they occur in narrow corridors  
46  
47 235 on palaeo-ice stream trunks (Evans et al., 2016). The spatial arrangement of the BI-SSb  
48  
49 236 geometrical ridge networks is identical to the wide arcuate zones of surge-related crevasse-  
50  
51 237 squeeze ridges found on modern glacier forelands, suggesting they may record a phase of  
52  
53 238 glacier surging by the BI-SSb lobe (see discussion).  
54  
55

56  
57 239  
58  
59  
60

1  
2  
3 240 **4.2 Subglacial landforms**

4  
5 241 **4.2.1 Glacial lineations**

6  
7  
8 242 Lineations occur in association with all five ice lobes, but vary in morphology from low-relief  
9  
10 243 flutings to prominent oval-shaped drumlins. For example, clusters of subdued flutings occur  
11  
12 244 around Bahía Inútil (Raedecke, 1978; Figure 3), whilst large swaths of rounded drumlins are  
13  
14 245 found in the Río Gallegos, Skyring, Otway and Magellan lobes. Of particular note are the  
15  
16 246 fields consisting of hundreds of elongate drumlins that occur in the outermost part of the Río  
17  
18 247 Gallegos lobe (Ercolano et al., 2004; Figure 9), around Laguna Cabeza del Mar in the Otway  
19  
20 248 lobe (Clapperton, 1989; Benn & Clapperton, 2000b; Figure 10C) and on the eastern side of  
21  
22 249 the Magellan Strait (Bentley et al., 2005; Lovell et al., 2012; Figure 4).

23  
24  
25 250 The precise genesis of glacial lineations is contentious, but it is generally agreed that they  
26  
27 251 are subglacially streamlined landforms related to the deformation and/or erosion of a soft  
28  
29 252 substrate by fast flowing glacier ice (Stokes et al., 2011). Hence, the lineations in our study  
30  
31 253 area were probably formed by subglacial deformation of glaciofluvial deposits during  
32  
33 254 advances of warm, wet-based ice (Clapperton, 1989; Benn & Clapperton, 2000b). Generally,  
34  
35 255 the lineations are associated with ice marginal features, but a few dense swaths of drumlins  
36  
37 256 occur in isolation from any apparent ice margin and show elements of convergence and  
38  
39 257 divergence, most clearly in the area around Laguna Cabeza del Mar in the Otway lobe  
40  
41 258 (Figure 2). Here, we suggest that the attenuated bedforms, parallel concordance and abrupt  
42  
43 259 lateral margins of the lineation patterns are similar to those in areas of former rapidly flowing  
44  
45 260 ice (Stokes & Clark, 1999, 2001; Evans et al., 2008; Lovell et al., 2012).

46  
47  
48 261

49  
50  
51 262 **4.2.2 Subdued moraine topography**

52  
53 263 Subdued moraine topography consists of low, arcuate changes in relief (> 1 km wide), often  
54  
55 264 over-printed by other moraine ridges or bands of smaller hummocky terrain. The features are  
56  
57 265 difficult to observe clearly on the ground and are best picked-out as positive relief in SRTM  
58  
59  
60

1  
2  
3 266 imagery or changes in vegetation in Landsat imagery. Subdued moraine topography is  
4  
5 267 predominantly found in the centre of the BI-SSb lobe and is fragmented in a regular pattern  
6  
7 268 north of Laguna Larga (Raedecke, 1978; Figure 3B).  
8  
9

10 269 The regular fracturing of subdued moraine topography north of Laguna Larga could  
11  
12 270 represent linear en echelon deposits linked to crevassing (Raedecke, 1978). However, this is  
13  
14 271 unlikely because the topography is draped by younger features such as moraine ridges,  
15  
16 272 glacial lineations and smaller hummocky terrain. Another possibility is that the subdued  
17  
18 273 moraine topography is similar to the 'traction ribs' inferred beneath modern ice masses  
19  
20 274 (Sergienko & Hindmarsh, 2013) and palaeo-ice stream tracks in the southwestern  
21  
22 275 Laurentide Ice Sheet . Given the similarity in orientation to moraine ridges, however, the  
23  
24 276 most likely explanation is that this subdued topography resulted from ice-marginal moraines  
25  
26 277 that were subsequently overridden and moulded subglacially, similar to landforms  
27  
28 278 (overridden moraines) observed in Iceland (Krüger, 1994; Evans & Twigg, 2002; Evans &  
29  
30 279 Orton, 2015; Evans et al., 1999; Evans, 2009; Evans et al., 2015).  
31  
32

33 280  
34  
35

#### 36 281 *4.2.3 Irregular dissected ridges*

37

38 282 A series of disorganised ridges, in places intersected by meltwater channels, are found in  
39  
40 283 association with the Skyring and Río Gallegos lobes, most prominently to the southeast of  
41  
42 284 the large swath of drumlins oriented southeastward in the Río Gallegos lobe (Flow-set 1: FS  
43  
44 285 1; Figure 9). The origin of the features is unclear, although the largest group appears to be  
45  
46 286 situated at the intersection between the former Río Gallegos and Skyring ice lobes.  
47  
48

49 287 We suggest that the Río Gallegos lobe advanced first into the area, creating a drumlin field  
50  
51 288 and moraine ridges. Subsequently, the Río Gallegos lobe retreated and the Skyring lobe  
52  
53 289 advanced over the drumlins and moraines, causing subglacial deformation that resulted in  
54  
55 290 an irregular pattern of hills and meltwater channels. The stratigraphic order is indicated by  
56  
57 291 meltwater from the Skyring lobe draining into the Río Gallegos depression.  
58  
59  
60

1  
2  
3 292  
4  
5  
6 293**4.3 Glaciofluvial landforms**7  
8 294 *4.3.1 Meltwater channels*  
9  
10

11 295 The study area is dominated by meltwater features, including hundreds of sinuous channels.  
12  
13 296 In places, such as the outer moraines of the Skyring, Otway and Magellan lobes, the  
14  
15 297 channels flow between moraine ridges (Figure 2), but elsewhere, such as the BI-SSb  
16  
17 298 depression and inner parts of the Río Gallegos, Skyring, Otway and Magellan lobes,  
18  
19 299 meltwater channels are clearer than the associated moraines (Bentley et al., 2005). The  
20  
21 300 channels vary in size, from less than 50 m wide to more than 150 m wide, and are  
22  
23 301 sometimes associated with channels of outwash where ice overtopped topographic  
24  
25 302 constraints (e.g. northeast of the Skyring and Otway lobes or north of the BI-SSb lobe).  
26  
27  
28 303  
29  
30

31 304 *4.3.2 Outwash plains*  
32

33 305 Outwash plains were identified based on their relatively smooth, featureless appearance,  
34  
35 306 whose surfaces gently grade downslope from former ice margins. The plains are associated  
36  
37 307 with moraines and hummocky terrain in all of the ice lobes, and (where they are  
38  
39 308 unconstrained by topography) wide, open sandur plains grade eastward. A prominent  
40  
41 309 exception is the outwash plain originating from Laguna Blanca in the Skyring lobe (Figures 2  
42  
43 310 and 10), which trends south-eastward into the Strait of Magellan and surrounds a former  
44  
45 311 moraine belt associated with the Otway lobe (Lovell et al., 2012).  
46  
47

48 312 The extensive nature of the glaciofluvial features implies that all of the ice lobes produced  
49  
50 313 large quantities of meltwater during stillstands and retreat. Whilst meltwater channels and  
51  
52 314 outwash plains are abundant within the study area, features such as ice contact fans, pitted  
53  
54 315 outwash plains and eskers are not. Indeed, there is a notable absence of eskers associated  
55  
56 316 with the ice lobes, which might imply that meltwater was rarely routed into conduits at the  
57  
58  
59  
60

1  
2  
3 317 bed (perhaps draining into the substrate or maybe as a result of cold-based ice) or that there  
4  
5 318 was insufficient time for conduits to form (Storrar et al., 2014a, 2014b). Alternatively, ice-  
6  
7 319 walled deposition may have been restricted to englacial settings, in a similar fashion to the  
8  
9 320 receding lowland lobes of Iceland, where drainage bypasses overdeepenings and hence  
10  
11 321 eskers emerge on the surface of downwasting snouts (Spedding & Evans, 2002; Bennett et  
12  
13 322 al., 2010; Bennett & Evans, 2012). Such a scenario would result in tunnel fills being  
14  
15 323 significantly reworked during deglaciation and consequently difficult to identify in the  
16  
17 324 landform record.

18  
19  
20 325

## 21 22 23 326 **4.4 Proglacial lake landforms**

### 24 25 327 **4.4.1 Former shorelines**

26  
27  
28 328 Numerous fragmentary shorelines are found within ca. 10 m elevation of contemporary  
29  
30 329 coastal areas. In addition, continuous shorelines are found above 10 m and, further inland,  
31  
32 330 around Lago Balmaceda in the Río Gallegos lobe (Figure 1); Seno Skyring; Seno Otway  
33  
34 331 (Figure 2); Laguna Blanca in the Skyring lobe (Figure 10A); south of Primera Angostura in  
35  
36 332 the Strait of Magellan (Figure 4); and Bahía Inútil (Figure 3A). Whilst the Skyring, Otway,  
37  
38 333 Magellan and Bahía Inútil shorelines are generally within 30 m of present-day sea-level,  
39  
40 334 those around Lago Balmaceda and Laguna Blanca are substantially higher.

41  
42  
43 335 Our glacial reconstruction, combined with DEM modelling, and the occurrence of localised  
44  
45 336 palaeolacustrine sedimentary evidence, leads us to infer that these shorelines relate to a  
46  
47 337 total of six large proglacial lakes that existed at various times in the overdeepenings in front  
48  
49 338 of the former ice lobes. This reconstruction supports previous work on proglacial lake  
50  
51 339 reconstruction in the area (Porter et al., 1992; Clapperton et al., 1995; McCulloch et al.,  
52  
53 340 2005a; Sagredo et al., 2011; Stern et al., 2011; Lovell et al., 2012; Kilian et al., 2007, 2013).  
54  
55 341 The ice-marginal truncation of these shorelines suggests that they formed in front of the ice  
56  
57 342 lobes, likely during recession into their respective topographic basins/overdeepenings.

1  
2  
3 343  
4  
56 344 **5 Style and dynamics of Quaternary glaciation**  
78  
9 345 **5.1 Active temperate glacial landsystem**  
10

11 346 The majority of the glacial geomorphology in the study area can broadly be divided into three  
12  
13 347 landform assemblages: morainic, subglacial and glaciofluvial (Figure 11). The components  
14  
15 348 of each assemblage as well as their inter-relationships are consistent with an active  
16  
17 349 temperate glacial landsystem developed during the advance and retreat of the ice lobes  
18  
19 350 (Evans & Twigg, 2002). The warm-based active recession of this landsystem produces three  
20  
21 351 characteristic landform-sediment associations. Firstly, dump, push and squeeze moraines  
22  
23 352 composed of proglacial sediments mark the ice limit, sometimes displaying annual  
24  
25 353 signatures or evidence for stillstands that create stacked features (Price, 1970; Evans et al.,  
26  
27 354 1999; Evans & Twigg, 2002; Evans et al., 2015). Low amplitude ridges formed from  
28  
29 355 overridden push moraines may also be found, draped by glacial lineations and moraines.  
30  
31 356 Secondly, subglacially streamlined flutings and drumlins occur between these moraines.  
32  
33 357 Thirdly, extensive glaciofluvial landforms occur where meltwater flows away from the warm-  
34  
35 358 based ice front. These features include ice-contact and spillway-fed outwash fans; ice  
36  
37 359 marginal outwash tracts; kame terraces; pitted outwash and eskers (Evans & Twigg, 2002;  
38  
39 360 Evans, 2003b). Active temperate glaciers are also capable of constructing arcuate bands of  
40  
41 361 hummocky moraine during recession as a result of incremental stagnation, driven by pulses  
42  
43 362 of supraglacial debris (Eyles, 1979; Bennett & Evans, 2012). The geomorphology in the  
44  
45 363 central part of the BI-SSb lobe (Figure 11) displays many of the landforms associated with  
46  
47 364 an active temperate landsystem: moraines containing proglacially-thrust and folded  
48  
49 365 sediments; possible recessional push moraines; overridden moraines; flutings and drumlins;  
50  
51 366 and glaciofluvial meltwater channels and outwash plains.

52  
53  
54  
55 367 The similarity between the landform assemblages in our study area and those associated  
56  
57 368 with active temperate glaciers supports the assertion that the ice lobes dominantly operated  
58  
59  
60

1  
2  
3 369 under an active temperate glacial landsystem. This is especially clear in the geomorphology  
4  
5 370 of the central BI-SSb lobe. The other ice lobes show the characteristics associated with  
6  
7 371 active temperate glaciers, but the geomorphology is either not as well preserved (as in the  
8  
9 372 Río Gallegos and Magellan lobes) or the moraines are more tightly nested (as in the Skyring  
10  
11 373 and Otway lobes) so that the assemblages are not as clear. Tightly nested moraine  
12  
13 374 sequences may indicate that the Skyring and Otway lobes retreated more slowly than the  
14  
15 375 other ice lobes, although there are no chronological constraints on the rate of this recession  
16  
17 376 (see Section 6.2). Similar patterns of tightly nested features have been observed in Iceland  
18  
19 377 (Bradwell et al., 2013), but, in our study, the cause may be related to topographic  
20  
21 378 constraints, rather than annual cycles in retreat (Kaplan et al., 2009; Anderson et al., 2012;  
22  
23 379 Barr & Lovell, 2014). Hence, the landform assemblages of the Skyring and Otway lobes may  
24  
25 380 be indicative of an active temperate landsystem, but they are not as clear as the BI-SSb lobe  
26  
27 381 due to slower glacier recession.

## 30 382 **5.2 External forcing of glacier behaviour**

31  
32  
33 383 There are a number of implications associated with our interpretation of an active temperate  
34  
35 384 glacial landsystem. Principally, Benn & Clapperton (2000a, 2000b) suggested that the  
36  
37 385 Magellan lobe operated under subpolar conditions, with a cold-based margin, during the  
38  
39 386 gLGM. By contrast, Bentley et al. (2005) advocated warm-based conditions extending to the  
40  
41 387 ice margin based on different glacier limits that implied steeper ice surface gradients. The  
42  
43 388 presence of proglacially thrust moraines and arcuate bands of hummocky terrain, if they  
44  
45 389 originated as controlled ridges (*sensu* Evans, 2009), are consistent with cold-based ice or at  
46  
47 390 least a polythermal basal regime (Benn & Clapperton, 2000b; Evans, 2009). Evidence for  
48  
49 391 glacial lineations extending to individual moraine ridges is a landform association indicative  
50  
51 392 of warm-based ice throughout the snout (Evans & Twigg, 2002; Evans, 2003b), and arcuate  
52  
53 393 hummocky terrain bands set within recessional push moraines are consistent with phases of  
54  
55 394 incremental stagnation by temperate glaciers. However, glacial thermal regimes form a  
56  
57 395 continuum upon which the landsystem signatures of polythermal glaciers, with frozen snouts  
58  
59  
60

1  
2  
3 396 (e.g. Svalbard valley glaciers and Icelandic upland icefields), and active temperate glaciers,  
4  
5 397 with winter frozen toe zones and pulsed supraglacial debris transfer, would be difficult to  
6  
7 398 differentiate (Evans, 2009). Particularly significant for southernmost Patagonia is the  
8  
9 399 independent evidence for permafrost conditions at the gLGM (Benn & Clapperton, 2000a,  
10  
11 400 2000b; Bockheim et al., 2009). Therefore, we suggest that the former ice lobes were  
12  
13 401 predominantly active temperate in nature, but were subject to periods of polythermal  
14  
15 402 conditions, thereby giving rise to phases of controlled moraine construction. A similar  
16  
17 403 scenario has been proposed for the southern limits of the Laurentide Ice Sheet in the interior  
18  
19 404 plains of North America (Clayton et al., 2001; Colgan et al., 2003; Bauder et al., 2005; Evans  
20  
21 405 et al., 2006, 2014). This further illustrates the importance of recognising what Evans (2013)  
22  
23 406 identifies as landsystem superimposition and spatio-temporal change, whereby changes in  
24  
25 407 the climatic environment occupied by a glacier will inevitably be reflected in its geomorphic  
26  
27 408 signature. The incremental stagnation versus controlled origin of the hummocky terrain arcs  
28  
29 409 is important to the palaeoglaciological reconstruction and its palaeoclimatic inferences made  
30  
31 410 above, and therefore needs to be vigorously tested by future sedimentological investigations.  
32  
33

34 411 The complex landform-sediment signatures of the southernmost Patagonian outlet lobes are  
35  
36 412 indicative of active temperate glaciers. Such glaciers are characterised by active advance  
37  
38 413 during periods of overall recession, primarily controlled by regional climatic variability  
39  
40 414 (Colgan et al., 2003; Evans, 2003b, 2011; Evans & Orton, 2015; Evans et al., 2015). Modern  
41  
42 415 examples include Breiðamerkurjökull, Fjallsjökull, Heinabergsjökull, Skalafellsjökull and  
43  
44 416 Fláajökull in Iceland (Evans & Twigg, 2002; Evans et al., 2015; Evans & Orton, 2015; Evans,  
45  
46 417 2003b). Both topographic control (Kaplan et al., 2009; Anderson et al., 2012; Barr & Lovell,  
47  
48 418 2014) and internal ice dynamics (Benn & Clapperton, 2000a, 2000b; Lovell et al., 2012) have  
49  
50 419 also been proposed as factors controlling glacial activity within this region. Our  
51  
52 420 geomorphological evidence implies that, for the majority of ice fluctuations, these internal  
53  
54 421 forcing factors may have been of secondary importance to climatic variability.  
55  
56

57 422  
58  
59  
60

1  
2  
3 423 **5.3 Internal forcing of glacier behaviour**  
4

5 424 Whilst the landform evidence suggests that the ice lobes predominantly advanced and  
6  
7 425 retreated according to an externally-forced active temperate landsystem, there is also  
8  
9 426 evidence for periods of rapid ice flow and proglacial lake development. Both of these  
10  
11 427 situations may have temporarily interrupted the primary climatic driver of glacial activity.  
12

13  
14 428 **5.3.1 Transient rapid ice flow**  
15

16  
17 429 A large swath of elongated, closely-spaced drumlins in the inner part of the Otway lobe  
18  
19 430 around Laguna Cabeza del Mar (FS 8 in Figure 12) has previously been hypothesised to  
20  
21 431 represent rapid ice flow (Benn & Clapperton, 2000b; Lovell et al., 2012). Unlike other glacial  
22  
23 432 lineations in the study area, this drumlin field resembles a terrestrial palaeo-ice stream, with  
24  
25 433 convergent flowlines, attenuated bedforms and abrupt lateral margins (Stokes & Clark, 1999;  
26  
27 434 Clark & Stokes, 2003; Lovell et al., 2012). Additionally, Lovell et al. (2012) raised the  
28  
29 435 possibility for surge-like behaviour of the Otway lobe based partly on this landform evidence.  
30  
31 436 Our study confirms that many of the landforms associated with surging activity are exhibited  
32  
33 437 in the study area, including thrust moraines, highly elongate flutings, hummocky terrain and  
34  
35 438 crevasse-squeeze ridges, which are often viewed as diagnostic of surge activity (Evans &  
36  
37 439 Rea, 1999, 2003; Schomacker et al., 2014; Lovell et al., 2015). As such, we suggest the ice  
38  
39 440 lobes may have periodically displayed rapid ice-flow and possible surge-like behaviour.  
40

41  
42 441 Our reconstruction of fast-flowing ice would have affected ice dynamics in parts of the ice  
43  
44 442 lobes. Similar fast-flowing systems in northern Patagonia during the gLGM are hypothesised  
45  
46 443 to have resulted in greater ice discharge rates (Glasser & Jansson, 2005), and rapid ice flow  
47  
48 444 across much of the eastern portion of the Patagonian Ice Sheet may help to explain  
49  
50 445 mismatches between model outputs and landform reconstructions (Hulton et al., 2002;  
51  
52 446 Glasser & Jansson, 2005). The presence of landforms linked to possible surge-like  
53  
54 447 advances further implies that, at times, the ice lobes may have briefly advanced in response  
55  
56 448 to non-climatic forcing. The possible evidence for palaeo-surges warrants further research,  
57  
58  
59  
60

1  
2  
3 449 particularly given the paucity of examples of surging systems in the palaeo-record and the  
4  
5 450 fact that some contemporary active temperate glaciers, such as Breiðamerkurjökull, have  
6  
7 451 also displayed surging activity and this is recorded in landsystem overprinting (Evans &  
8  
9 452 Twigg, 2002).

10  
11  
12 45313  
14  
15 454 *5.3.2 Proglacial lake development*

16  
17 455 The clearest proglacial lake landforms are within the Skyring lobe, where meltwater  
18  
19 456 accumulated above the present day Laguna Blanca. Shorelines and DEM modelling indicate  
20  
21 457 a maximum lake surface elevation of ca. 190 m.a.s.l., which drained northward into the basin  
22  
23 458 previously occupied by the Río Gallegos lobe (Lovell et al., 2012; Figure 10A and B). This  
24  
25 459 reconstruction is supported by sedimentological evidence northeast of Laguna Blanca  
26  
27 460 consisting of rhythmically laminated silt and clay sediments, containing dropstones (Figure  
28  
29 461 10E). Our ice limit for the Otway lobe differs from Lovell et al. (2012), such that a similar  
30  
31 462 proglacial lake did not form in front of the Otway lobe because meltwater could drain  
32  
33 463 southeastward in front of the Magellan lobe. Once the Skyring lobe retreated beyond the  
34  
35 464 topographic bluff separating it from the Otway lobe, drainage of the palaeo-Laguna Blanca  
36  
37 465 proglacial lake switched from a northward to a south-eastward direction, in front of the Otway  
38  
39 466 and Magellan lobes and into the Strait of Magellan (Figure 10C and F). The drainage  
40  
41 467 resulted in the formation of large meltwater channels and an associated outwash plain that  
42  
43 468 surrounded a moraine belt associated with the Otway lobe.

44  
45  
46 469 Proglacial lakes are also reconstructed in front of the BI-SSb and Magellan lobes (Figure  
47  
48 470 13), consistent with the presence of lacustrine sediments (McCulloch et al., 2005a). The BI-  
49  
50 471 SSb lake reached approximately 20 m.a.s.l. before draining at Onaisín, eastward toward the  
51  
52 472 Atlantic through a channel now marked by Laguna Larga (Figure 3A and B). Likewise the  
53  
54 473 Magellan lake drained eastward toward the Atlantic, but the height of the lake is less clear as  
55  
56 474 the drainage channel is below present day sea-level (Porter et al., 1992; Clapperton et al.,  
57  
58  
59  
60

1  
2  
3 475 1995; McCulloch et al., 2005a). Our reconstruction suggests that at its peak the lake  
4  
5 476 extended onto the low plain in front of the Otway lobe. Small lakes also formed at 10-20  
6  
7 477 m.a.s.l. on the eastern flank of the Magellan lobe, north of Porvenir (Figure 4B). One of  
8  
9 478 these lakes deposited a large section of rhythmically laminated silt and clay sediments at  
10  
11 479 Laguna Verde (Figures 10G, H, I and 4B).

12  
13  
14 480 A proglacial lake formed in front of the Otway lobe once ice had retreated into the present-  
15  
16 481 day Seno Otway, and there is evidence for a channel initially draining north-eastward into  
17  
18 482 the Strait of Magellan (Mercer, 1976; McCulloch et al., 2005a). However, once the lake level  
19  
20 483 dropped to around 20 m.a.s.l., drainage would have switched to the northwest through Canal  
21  
22 484 Fitzroy into a similar lake at 10-20 m.a.s.l. within present-day Seno Skyring (Figure 2). The  
23  
24 485 Skyring proglacial lake drained northward through Estero Obstrucción (Figure 1) into a large  
25  
26 486 lake in front of the Río Gallegos lobe, the extent of which is unclear (Sagredo et al., 2011;  
27  
28 487 Stern et al., 2011), although final drainage of the Otway, Skyring and Río Gallegos lakes  
29  
30 488 would have been westward through Golfo Almirante Montt (Figure 1) once ice had receded  
31  
32 489 into the mountains (McCulloch et al., 2005a; Stern et al., 2011).

33  
34  
35 490 Former proglacial lakes would also have affected glacial dynamics by promoting increased  
36  
37 491 rates of ice retreat (Porter et al., 1992; Teller, 2003; Lovell et al., 2012; Carrivick & Tweed,  
38  
39 492 2013). The presence of a proglacial lake at the margin of a glacier can trigger positive  
40  
41 493 feedbacks such as increased englacial water pressure and temperature; increased  
42  
43 494 subglacial pressure; and increased ice surface gradients, which can result in calving, ice-  
44  
45 495 margin flotation and the flushing of sediment from beneath the ice (Carrivick & Tweed,  
46  
47 496 2013). This results in greater ice mass loss and glacial draw-down (Lovell et al., 2012).  
48  
49 497 Porter et al. (1992) also suggested that calving of the Magellan and BI-SSb lobes could have  
50  
51 498 resulted in a rapid loss of ice. Given the potential importance of proglacial lakes in controlling  
52  
53 499 ice dynamics within this region, future work should aim to better constrain their evolution  
54  
55 500 over time.

## 501 **6 Glacial reconstruction and timing**

### 502 **6.1 Glacial limits and flow-sets**

503 Three sets of ice-marginal landforms were used to demarcate former glacial limits: morainic  
504 landforms (including hummocky terrain), glacial lineation flow-sets (see below), and  
505 meltwater channels. The different lines of evidence yielded a consistent pattern and the data  
506 were synthesised to create a map of prominent limits for each ice lobe (Figure 12). Many of  
507 these limits corroborate previous work defining glacial limits in the region (Meglioli, 1992;  
508 Clapperton et al., 1995; Coronato et al., 2004; Bentley et al., 2005; Lovell et al., 2012), but  
509 the wider scope of our mapping reveals a more detailed pattern than has been previously  
510 reported. For comparison, we also included less extensive limits from Kilian et al. (2007) for  
511 the Skyring lobe (Figure 12D).

512 A total of 20 flow-sets (FS) were identified within the study area (Figure 12B), with those of  
513 the Skyring and Otway lobes similar to Lovell et al. (2012). An exception is the separation of  
514 FS 7 and 8 based on differing morphology: the drumlins around Laguna Cabeza del Mar are  
515 noticeably longer, wider, and higher than the long flutings further to the northeast. This  
516 division is important because FS 8 corresponds with moraines dissecting the Otway  
517 depression. Some flow-sets within the inner parts of the Río Gallegos, Skyring, Magellan  
518 and BI-SSb lobes have been discussed in previous studies (Benn & Clapperton, 2000b;  
519 Ercolano et al., 2004; Bentley et al., 2005; Lovell et al., 2012), but the outer flow-sets of the  
520 Río Gallegos and BI-SSb lobes have not been reported previously.

521 The glacial limits that we have defined can be used to reconstruct a relative sequence of  
522 events in the glacial history, enhanced by information about ice dynamics from our  
523 landsystems approach. Correlating between the limits of adjacent ice lobes can be  
524 problematic because they are generally reconstructed from fragmentary records, and joining-  
525 up limits can over-emphasise correlation without robust chronological controls. However, in  
526 places, our approach informs the relative timing of advance and retreat between lobes based

1  
2  
3 527 on cross-cutting landform assemblages. Using cross-cutting relationships between flow-sets  
4  
5 528 and ice marginal landform assemblages, we identify eight separate relative time steps in our  
6  
7 529 reconstruction (Figure 13). These time steps are shown in relation to present-day basal  
8  
9 530 topography and the height of former proglacial lakes in Figure 14. We now briefly discuss  
10  
11 531 key aspects of the nature and timing of this glacial history in relation to the eight time steps  
12  
13 532 and a compilation of recalibrated chronological information (Figure 15).

## 16 533 **6.2 Chronological framework**

17  
18 534 This study is principally engaged with reconstructing the dynamics of former ice lobes  
19  
20 535 without considering time-dependent variation. However, it is possible and informative to  
21  
22 536 place our time steps within a framework of previously published chronological data (Figures  
23  
24 537 13 and 15). Full details of this chronological compilation, including calibration and  
25  
26 538 recalculation methods, are given in the Supplementary Material and Tables S1, S2, S3 and  
27  
28 539 S4.

### 31 540 **6.2.1 Time steps 1-4: Pre-gLGM advances**

32  
33  
34 541 There is uncertainty regarding the ages of pre-gLGM glacial limits within the study area (time  
35  
36 542 steps 1-4 in our reconstruction). Cosmogenic nuclide exposure dating of boulders from  
37  
38 543 moraines of the BI-SSb, Magellan and Río Gallegos lobes (Kaplan et al., 2007; Evenson et  
39  
40 544 al., 2009) has yielded ages that are substantially younger than associated  $^{40}\text{Ar}/^{39}\text{Ar}$  dates  
41  
42 545 from nearby volcanic flows (Figure 13A, B and C; (Meglioli, 1992; Singer et al., 2004), the  
43  
44 546 cause of which is contentious (Kaplan et al., 2007; Darvill et al., 2015a). Darvill et al. (2015b)  
45  
46 547 used  $^{10}\text{Be}/^{26}\text{Al}$  depth profiles through outwash sediments to show that two limits previously  
47  
48 548 assigned to older glacial stages were deposited during the last glacial cycle. Overall, the  
49  
50 549 large spread of boulder ages associated with time steps 1-4 may result from post-  
51  
52 550 depositional processes such as boulder erosion (Kaplan et al., 2007) and the gradual melt-  
53  
54 551 out of dead ice in hummocky terrain (Schomacker, 2008; Darvill et al., 2015a).

1  
2  
3 552 In time step 4, the BI-SSb lobe re-advanced to close to the limit of time step 3 (Figure 14),  
4  
5 553 with  $^{10}\text{Be}$  dates from boulders of 24.3 ka and 224.1 ka (Figures 13D; Kaplan et al., 2007). A  
6  
7 554 depth-profile through associated outwash yielded a more robust age of 30.1 ka (Darvill et al.,  
8  
9 555 2015b). For the Magellan lobe, eight  $^{10}\text{Be}$  ages between 24.8 ka and 36.9 ka and two  $^{26}\text{Al}$   
10  
11 556 ages of 31.0 ka and 32.6 ka (Kaplan et al., 2007) imply that the limit may have been  
12  
13 557 deposited at a similar time to that of the BI-SSb lobe (Figure 15).

#### 14 15 16 558 *6.2.2 Time steps 5-6: Re-advances, rapid flow and lake drainage*

17  
18 559 The Otway lobe re-advanced significantly during time step 5 (Figure 13E), forming FS 8  
19  
20 560 around Laguna Cabeza del Mar and shifting the ice divide between the Otway and Magellan  
21  
22 561 lobes south-eastward into the present-day Strait of Magellan. The BI-SSb lobe also re-  
23  
24 562 advanced to a limit close to Bahía San Sebastián, depositing a large terminal moraine that is  
25  
26 563 still preserved east of Laguna Larga (Figure 3) and forming FS 17 (Figure 13E). The re-  
27  
28 564 advances of these two ice lobes may have been in response to rapid ice flow (and possible  
29  
30 565 surge-like activity based on the presence of thrust moraines, highly elongate flutings,  
31  
32 566 hummocky terrain and crevasse-squeeze ridges). The Río Gallegos, Magellan and Skyring  
33  
34 567 lobes retreated during time step 5, with the latter developing a proglacial lake – palaeo-  
35  
36 568 Laguna Blanca – which may have further facilitated ice loss through calving (Figures 13E  
37  
38 569 and 14). However, there are no direct age constraints for this time step. Recession  
39  
40 570 continued during time step 6, allowing the potentially catastrophic drainage of palaeo-  
41  
42 571 Laguna Blanca from in front of the Skyring lobe east to south-easterly in front of the Otway  
43  
44 572 and Magellan lobes (Figure 13F). The drainage event is important because it acts as a  
45  
46 573 stratigraphic tie-point for all three ice lobes (Figure 15). As mentioned in Section 6.2.1, ages  
47  
48 574 of 24.8 ka and 36.9 ka for the Magellan lobe at Primera Angostura (Figure 2) suggest that it  
49  
50 575 advanced prior to the gLGM during the last glacial cycle. The lake drainage is constrained by  
51  
52 576 these ages and four more  $^{10}\text{Be}$  ages of 27.4 ka to 29.9 ka on Península Juan Mazía  
53  
54  
55 577 (McCulloch et al., 2005b; Kaplan et al., 2008a). The implication is that the Skyring, Otway  
56  
57  
58  
59  
60

1  
2  
3 578 and Magellan lobes were all retreating from more extensive positions prior to the gLGM  
4  
5 579 (Figure 15).  
6

7  
8 580 *6.2.3 Time step 7: The gLGM*  
9

10 581 During time step 7, the ice lobes reached positions that have been broadly correlated with  
11  
12 582 the gLGM (Figures 13G and 15). Based upon our landform evidence (e.g. highly elongate  
13  
14 583 flutings and hummocky terrain), the Magellan lobe readvance may have been surge-like, and  
15  
16 584 has been  $^{10}\text{Be}$  dated to between 18.3 ka and 23.2 ka. The BI-SSb lobe readvance has also  
17  
18 585 been  $^{10}\text{Be}$ ,  $^{26}\text{Al}$  and  $^{36}\text{Cl}$  dated to between 15.6 ka and 55.8 ka (though sixteen  $^{10}\text{Be}$  dates  
19  
20 586 were between 17.6 ka and 24.9 ka; McCulloch et al., 2005b; Kaplan et al., 2007, 2008a;  
21  
22 587 Evenson et al., 2009). The reason for the scatter in ages is unclear, although the  $^{10}\text{Be}$  date  
23  
24 588 of 55.8 ka may be due to inheritance, given that most of the dates are from a large erratic  
25  
26 589 boulder train on the south-eastern side of Bahía Inútil (Darvill et al., 2015a). There are no  
27  
28 590 supporting ages for the Río Gallegos, Skyring and Otway lobes but they were likely situated  
29  
30 591 within the present-day fjords.  
31

32  
33 592 *6.2.4 Time step 8: Rapid retreat*  
34

35  
36 593 All of the ice lobes were in post-gLGM retreat during time step 8 (Figure 13H), developing  
37  
38 594 proglacial lakes in front of their receding margins that likely increased the rate of ice loss  
39  
40 595 through calving (Figure 14; Porter et al., 1992; Kilian et al., 2007; Carrivick & Tweed, 2013).  
41  
42 596 The Magellan and BI-SSb proglacial lakes drained eastward toward the Atlantic, although  
43  
44 597 their extent is uncertain. Drainage of the Otway proglacial lake initially occurred east to  
45  
46 598 north-eastward into the Magellan lake, but as lake levels dropped during ice retreat,  
47  
48 599 drainage switched to north-westward into the Skyring proglacial lake, cutting the Fitzroy  
49  
50 600 channel (McCulloch et al., 2005a; Kilian et al., 2013). In turn, the Skyring proglacial lake  
51  
52 601 drained into the Río Gallegos proglacial lake that, by this time, may have drained westward  
53  
54 602 into the Pacific Ocean through ice-free fjords dissecting the Andes (McCulloch et al., 2005a;  
55  
56 603 Kilian et al., 2013). It is possible that Río Gallegos ice was still extensive, such that drainage  
57  
58  
59  
60

1  
2  
3 604 occurred in a southwards direction, reaching the Pacific through Seno Otway (Stern et al.,  
4  
5 605 2011). Ultimately, uncertainty in the configuration of the Río Gallegos lobe makes it difficult  
6  
7 606 to assess drainage routes.  
8  
9

10 607 Ice-free conditions in Seno Skyring and Seno Otway have been dated to at least 14.8 ka and  
11  
12 608 14.7 ka, respectively, based on radiocarbon dating and tephrostratigraphy of sediment cores  
13  
14 609 (Kilian et al., 2013). The Skyring lobe may have been undergoing rapid retreat linked in part  
15  
16 610 to calving (Kilian et al., 2007). Numerous radiocarbon dates suggest that retreat of the  
17  
18 611 Magellan and BI-SSb ice lobes was also under way by at least 14-15 ka (Porter et al., 1992;  
19  
20 612 Anderson & Archer, 1999; Clapperton et al., 1995; McCulloch & Bentley, 1998; McCulloch et  
21  
22 613 al., 2005b), although the presence of the Reclús tephra within lake sediments implies that  
23  
24 614 full retreat and final proglacial lake drainage cannot have been before *ca.* 14.3 ka  
25  
26 615 (McCulloch et al., 2005a). The rapid retreat, and possible collapse, of the BI-SSb lobe is  
27  
28 616 supported by radiocarbon dates as early as 16.8 ka in central Cordillera Darwin (Hall et al.,  
29  
30 617 2013; Figure 15). A similarly rapid retreat is reconstructed for the Magellan lobe (Figure 15),  
31  
32 618 likely linked to the broad calving termini of these ice lobes (Porter et al., 1992).  
33  
34

35 619

## 36 37 38 620 **7 Conclusions**

39  
40  
41 621 This study presents a reconstruction of the relative history of five former ice lobes in  
42  
43 622 southernmost South America. We reconstruct eight time steps, which highlight the dynamic  
44  
45 623 nature of this part of the ice sheet margin, and use a landsystem approach to show that the  
46  
47 624 ice lobes dominantly displayed behaviour similar to active temperate glaciers. This involved  
48  
49 625 warm-based ice actively re-advancing during overall retreat of the ice margin and questions  
50  
51 626 previous hypotheses that the ice lobes displayed sub-polar characteristics with cold-based  
52  
53 627 margins. The implication is that active temperate ice lobes would have been primarily  
54  
55 628 controlled by regional climate variability. Superimposed on these active temperate  
56  
57 629 landsystems are areas where swaths of elongated, closely-spaced drumlins and suites of  
58  
59  
60

1  
2  
3 630 landforms including possible crevasse-squeeze ridges suggest periodically rapid ice flow,  
4  
5 631 perhaps indicative of some readvances linked to surge-like activity. Additionally, our  
6  
7 632 reconstruction highlights the importance of the palaeo-Laguna Blanca proglacial lake, which  
8  
9 633 developed in front of the Skyring lobe, and drained, potentially catastrophically, prior to the  
10  
11 634 gLGM. The development of other proglacial lakes in front of all of the ice lobes following the  
12  
13 635 gLGM would have promoted calving and rapid retreat, or collapse, of the ice margins.

14  
15  
16 636 For the Río Gallegos, Skyring and Otway lobes, existing age constraints are scarce and  
17  
18 637 contradictory, but our recalculation of dates for older positions of the Magellan lobe suggests  
19  
20 638 that at least one limit of greater extent than the gLGM limit was deposited around 30 ka. This  
21  
22 639 suggests that the BI-SSb and Magellan lobes advanced in a similar manner and at similar  
23  
24 640 times. Similarity in the timing of ice advances from the available chronological information  
25  
26 641 implies that, broadly speaking, ice lobe response was primarily controlled by climate  
27  
28 642 variability, supporting a model of active temperate glaciation. However, additional  
29  
30 643 chronological controls are needed to test this model further, particularly for the Río Gallegos,  
31  
32 644 Skyring and Otway lobes.

33  
34  
35 645

## 36 37 38 646 **8 Acknowledgments**

39  
40  
41 647 CMD would like to thank Will Christiansen, Mark Hulbert and Paul Lincoln for their  
42  
43 648 assistance and companionship in the field, as well as Jorge Rabassa, Andrea Coronato and  
44  
45 649 Juan Carlos Aravena for fieldwork support and guidance. This research was funded by a UK  
46  
47 650 NERC Ph.D. studentship (NE/j500215/1) awarded to CMD at Durham University. Fieldwork  
48  
49 651 was also supported by an Explorers Club Exploration Grant, Quaternary Research  
50  
51 652 Association NRW Award, Santander Mobility Grant, the Durham University Faculty of Social  
52  
53 653 Sciences and Health, Durham University Geography Department, and a UK NERC Ph.D.  
54  
55 654 studentship (NE/I528050/1) awarded to HL at Queen Mary University of London.  
56  
57 655 Additionally, the Ph.D. research of CMD was assisted by a Royal Geographical Society  
58  
59  
60

1  
2  
3 656 Dudley Stamp Memorial Award and British Society for Geomorphology Postgraduate  
4  
5 657 Research Grant, as well as funding from the Norman Richardson Postgraduate Research  
6  
7 658 Fund and an Ustinov College Travel Grant at Durham University. We are grateful to Neil  
8  
9 659 Glasser for comments on an early version of this manuscript and to Andrew Lorrey for his  
10  
11 660 editorial work on the published version. This paper benefitted greatly from the detailed and  
12  
13 661 considered comments of three anonymous reviewers.

14  
15  
16 662

17  
18  
19 663 **9 References**

- 20  
21  
22 664 Aber, J. (1985). The character of glaciotectionism. *Geologie en Mijnbouw* **64**, 389–395.  
23  
24 665 Aber, J., Croot, D. & Fenton, M. (1989). *Glaciotectonic Landforms and Structures*. Dordrecht:  
25 666 Kluwer Academic Publishers.  
26 667 Anderson, D.M. & Archer, R.B. (1999). Preliminary evidence of early deglaciation in southern  
27 668 Chile. *Palaeogeography Palaeoclimatology Palaeoecology* **146** (1-4), 295–301.  
28  
29 669 Anderson, R.S., Dühnforth, M., Colgan, W. & Anderson, L. (2012). Far-flung moraines:  
30 670 Exploring the feedback of glacial erosion on the evolution of glacier length.  
31 671 *Geomorphology* **179**, 269–285.  
32 672 Attig, J.W., Mickelson, D.M. & Clayton, L. (1989). Late Wisconsin landform distribution and  
33 673 glacier-bed conditions in Wisconsin. *Sedimentary Geology* **62** (2-4), 399–405.  
34  
35 674 Barr, I.D. & Lovell, H. (2014). A review of topographic controls on moraine distribution.  
36 675 *Geomorphology* **226**, 44–64.  
37 676 Bauder, A., Mickelson, D.M. & Marshall, S.J. (2005). Numerical modeling investigations of the  
38 677 subglacial conditions of the southern Laurentide ice sheet. *Annals of Glaciology* **40**  
39 678 (1987), 219–224.  
40  
41 679 Benn, D.I. (1992). The genesis and significance of ‘hummocky moraine’: Evidence from the  
42 680 Isle of Skye, Scotland. *Quaternary Science Reviews* **11** (7-8), 781–799.  
43  
44 681 Benn, D.I. & Clapperton, C.M. (2000a). Glacial sediment-landform associations and  
45 682 paleoclimate during the last glaciation, Strait of Magellan, Chile. *Quaternary Research*  
46 683 **54** (1), 13–23.  
47 684 Benn, D.I. & Clapperton, C.M. (2000b). Pleistocene glaciotectionic landforms and sediments  
48 685 around central Magellan Strait, southernmost Chile: evidence for fast outlet glaciers  
49 686 with cold-based margins. *Quaternary Science Reviews* **19** (6), 591–612.  
50  
51 687 Bennett, G.L. & Evans, D.J.A. (2012). Glacier retreat and landform production on an  
52 688 overdeepened glacier foreland: the debris-charged glacial landsystem at Kvíárjökull,  
53 689 Iceland. *Earth Surface Processes and Landforms* **37** (15), 1584–1602.  
54  
55 690 Bennett, G.L., Evans, D.J.A., Carbonneau, P. & Twigg, D.R. (2010). Evolution of a debris-  
56 691 charged glacier landsystem, Kvíárjökull, Iceland. *Journal of Maps* **6** (1), 40–67.  
57 692 Bennett, M.R., Hambrey, M.J., Huddart, D. & Ghienne, J.F. (1996). The formation of a  
58  
59  
60

- 1  
2  
3 693 geometrical ridge network by the surge-type glacier Kongsvegen, Svalbard. *Journal of*  
4 694 *Quaternary Science* **11** (6), 437–449.
- 5 695 Bentley, M.J., Sugden, D.E., Hulton, N.R.J. & McCulloch, R.D. (2005). The landforms and  
6 696 pattern of deglaciation in the Strait of Magellan and Bahia Inútil, southernmost South  
7 697 America. *Geografiska Annaler Series a-Physical Geography* **87A** (2), 313–333.
- 8  
9 698 Blomdin, R., Murray, A., Thomsen, K.J., Buylaert, J.-P., Sohbati, R., Jansson, K.N. &  
10 699 Alexanderson, H. (2012). Timing of the deglaciation in southern Patagonia: Testing the  
11 700 applicability of K-Feldspar IRSL. *Quaternary Geochronology* **10** (0), 264–272.
- 12  
13 701 Bockheim, J., Coronato, A., Rabassa, J., Ercolano, B. & Ponce, J. (2009). Relict sand  
14 702 wedges in southern Patagonia and their stratigraphic and paleo-environmental  
15 703 significance. *Quaternary Science Reviews* **28** (13-14), 1188–1199.
- 16  
17 704 Boulton, G.S. (1972). Modern Arctic glaciers as depositional models for former ice sheets.  
18 705 *Journal of the Geological Society* **128** (4), 361–393.
- 19 706 Bradwell, T., Sigurdsson, O. & Everest, J. (2013). Recent, very rapid retreat of a temperate  
20 707 glacier in SE Iceland. *Boreas* **42** (4), 959–973.
- 21  
22 708 Caldenius, C.C. zo. (1932). Las Glaciaciones Cuaternarias en la Patagonia y Tierra del  
23 709 Fuego. *Geografiska Annaler* **14**, 1–164.
- 24 710 Caniupán, M., Lamy, F., Lange, C.B., Kaiser, J., Arz, H., Kilian, R., Baeza Urrea, O.,  
25 711 Aracena, C., Hebbeln, D., Kissel, C., Laj, C., Mollenhauer, G. & Tiedemann, R. (2011).  
26 712 Millennial-scale sea surface temperature and Patagonian Ice Sheet changes off  
27 713 southernmost Chile (53°S) over the past 60 kyr. *Paleoceanography* **26** (3), n/a–n/a.
- 28  
29 714 Carrivick, J.L. & Tweed, F.S. (2013). Proglacial lakes: character, behaviour and geological  
30 715 importance. *Quaternary Science Reviews* **78**, 34–52.
- 31 716 Clapperton, C.M. (1989). Asymmetrical drumlins in Patagonia, Chile. *Sedimentary Geology*  
32 717 **62** (2–4), 387–398.
- 33  
34 718 Clapperton, C.M. (1993). *Quaternary geology and geomorphology of South America*. B.V.,  
35 719 Amsterdam: Elsevier Science Publishers.
- 36  
37 720 Clapperton, C.M., Sugden, D.E., Kaufman, D.S. & McCulloch, R.D. (1995). The Last  
38 721 Glaciation in Central Magellan Strait, southernmost Chile. *Quaternary Research* **44** (2),  
39 722 133–148.
- 40 723 Clark, C.D. (1999). Glaciodynamic context of subglacial bedform generation and  
41 724 preservation. *Annals of Glaciology* **28** (1), 23–32.
- 42  
43 725 Clark, C.D. & Stokes, C.R. (2003). Palaeo-ice stream landsystem. In: D. J. A. Evans (ed.).  
44 726 *Glacial Landsystems*. 204–227, London: Hodder Arnold.
- 45 727 Clark, P.U., Dyke, A.S., Shakun, J.D., Carlson, A.E., Clark, J., Wohlfarth, B., Mitrovica, J.X.,  
46 728 Hostetler, S.W. & McCabe, A.M. (2009). The Last Glacial Maximum. *Science* **325**  
47 729 (5941), 710–714.
- 48  
49 730 Clayton, L. (1964). Karst topography on stagnant glaciers. *Journal of Glaciology* **5**, 107–112.
- 50  
51 731 Clayton, L., Attig, J.W. & Mickelson, D.M. (2001). Effects of late Pleistocene permafrost on  
52 732 the landscape of Wisconsin, USA. *Boreas* **30** (3), 173–188.
- 53 733 Colgan, P.M., Mickelson, D.M. & Cutler, P.M. (2003). Ice-marginal terrestrial landsystems:  
54 734 southern Laurentide Ice Sheet margin. In: D. J. A. Evans (ed.). *Glacial Landsystems*.  
55 735 111–142, London: Hodder Arnold.
- 56  
57 736 Coronato, A., Martínez, O. & Rabassa, J. (2004). Glaciations in Argentine Patagonia,  
58 737 southern South America. In: J. Ehlers & P. L. Gibbard (eds.). *Developments in*

- 1  
2  
3 738 *Quaternary Sciences*. **2**, 49–67, Elsevier.
- 4 739 Coronato, A.M.J., Coronato, F., Mazzoni, E. & Vázquez, M. (2008). The Physical Geography  
5 740 of Patagonia and Tierra del Fuego. In: J. Rabassa (ed.). *Developments in Quaternary*  
6 741 *Sciences*. **11**, 13–55, Elsevier.
- 7  
8 742 Darvill, C.M., Bentley, M.J. & Stokes, C.R. (2015a). Geomorphology and weathering  
9 743 characteristics of erratic boulder trains on Tierra del Fuego, southernmost South  
10 744 America: Implications for dating of glacial deposits. *Geomorphology* **228**, 382–397.
- 11 745 Darvill, C.M., Bentley, M.J., Stokes, C.R., Hein, A.S. & Rodés, Á. (2015b). Extensive MIS 3  
12 746 glaciation in southernmost Patagonia revealed by cosmogenic nuclide dating of  
13 747 outwash sediments. *Earth and Planetary Science Letters* **429**, 157–169.
- 14 748 Darvill, C.M., Stokes, C.R., Bentley, M.J. & Lovell, H. (2014). A glacial geomorphological  
15 749 map of the southernmost ice lobes of Patagonia: the Bahía Inútil – San Sebastián,  
16 750 Magellan, Otway, Skyring and Río Gallegos lobes. *Journal of Maps* **10** (3), 500–520.
- 17 751 Doughty, A.M., Schaefer, J.M., Putnam, A.E., Denton, G.H., Kaplan, M.R., Barrell, D.J.A.,  
18 752 Andersen, B.G., Kelley, S.E., Finkel, R.C. & Schwartz, R. (2015). Mismatch of glacier  
19 753 extent and summer insolation in Southern Hemisphere mid-latitudes. *Geology* **43** (5),  
20 754 407–410.
- 21 755 Douglass, D.C., Singer, B.S., Kaplan, M.R., Mickelson, D.M. & Caffee, M.W. (2006).  
22 756 Cosmogenic nuclide surface exposure dating of boulders on last-glacial and late-glacial  
23 757 moraines, Lago Buenos Aires, Argentina: Interpretive strategies and paleoclimate  
24 758 implications. *Quaternary Geochronology* **1** (1), 43–58.
- 25 759 Dyke, A.S. & Evans, D.J.A. (2003). Ice-marginal terrestrial landsystems: Northern Laurentide  
26 760 and Inuitian ice sheet margins. In: D. J. A. Evans (ed.). *Glacial Landsystems*. 143–  
27 761 165, London: Hodder Arnold.
- 28 762 Eaves, S.R., N. Mackintosh, A., Winckler, G., Schaefer, J.M., Alloway, B. V. & Townsend,  
29 763 D.B. (2016). A cosmogenic <sup>3</sup>He chronology of late Quaternary glacier fluctuations in  
30 764 North Island, New Zealand (39°S). *Quaternary Science Reviews* **132**, 40–56.
- 31 765 Ercolano, B., Mazzoni, E., Vazquez, M. & Rabassa, J. (2004). Drumlins and drumlinoid  
32 766 forms of the Lower Pleistocene in southern Patagonia, Province of Santa Cruz. *Rev.*  
33 767 *Asoc. Geol. Argent.* **59** (4), 771–777.
- 34 768 Etzelmüller, B., Hagen, J., Vatne, G., Ødegård, R. & Sollid, J. (1996). Glacial debris  
35 769 accumulation and sediment deformation influenced by permafrost: examples from  
36 770 Svalbard. *Annals of Glaciology* **22**, 53–62.
- 37 771 Evans, D.J.A. (2009). Controlled moraines: origins, characteristics and palaeoglaciological  
38 772 implications. *Quaternary Science Reviews* **28** (3–4), 183–208.
- 39 773 Evans, D.J.A. (2013). Geomorphology and Retreating Glaciers. In: R. Giardino & J. Harbor  
40 774 (eds.). *Treatise on Geomorphology*. 460–478, Elsevier.
- 41 775 Evans, D.J.A. (2003a). *Glacial Landsystems*. Hodder Arnold, London.
- 42 776 Evans, D.J.A. (2011). Glacial landsystems of Satujökull, Iceland: A modern analogue for  
43 777 glacial landsystem overprinting by mountain icecaps. *Geomorphology* **129** (3–4), 225–  
44 778 237.
- 45 779 Evans, D.J.A. (2003b). Ice marginal terrestrial landsystems: Active temperate glacier  
46 780 margins. In: D. J. A. Evans (ed.). *Glacial Landsystems*. 12–43, London: Hodder Arnold.
- 47 781 Evans, D.J.A., Archer, S. & Wilson, D.J.H. (1999). A comparison of the lichenometric and  
48 782 Schmidt hammer dating techniques based on data from the proglacial areas of some  
49 783 Icelandic glaciers. *Quaternary Science Reviews* **18** (1), 13–41.
- 50  
51  
52  
53  
54  
55  
56  
57  
58  
59  
60

- 1  
2  
3 784 Evans, D.J.A., Clark, C.D. & Rea, B.R. (2008). Landform and sediment imprints of fast  
4 785 glacier flow in the southwest Laurentide Ice Sheet. *Journal of Quaternary Science* **23**  
5 786 (3), 249–272.
- 6  
7 787 Evans, D.J.A., Ewertowski, M. & Orton, C. (2015). Fláajökull (north lobe), Iceland: active  
8 788 temperate piedmont lobe glacial landsystem. *Journal of Maps* 1–13.
- 9  
10 789 Evans, D.J.A. & Orton, C. (2015). Heinabergsjökull and Skalafellsjökull, Iceland: active  
11 790 temperate piedmont lobe and outwash head glacial landsystem. *Journal of Maps* **11** (3),  
12 791 415–431.
- 13  
14 792 Evans, D.J.A. & Rea, B.R. (1999). Geomorphology and sedimentology of surging glaciers: a  
15 793 land-systems approach. *Annals of Glaciology* **28** (1), 75–82.
- 16  
17 794 Evans, D.J.A. & Rea, B.R. (2003). Surging glacier landsystem. In: D. J. A. Evans (ed.).  
18 795 *Glacial Landsystems*. 259–288, London: Hodder Arnold.
- 19  
20 796 Evans, D.J.A., Rea, B.R., Hiemstra, J.F. & Ó Cofaigh, C. (2006). A critical assessment of  
21 797 subglacial mega-floods: a case study of glacial sediments and landforms in south-  
22 798 central Alberta, Canada. *Quaternary Science Reviews* **25** (13-14), 1638–1667.
- 23  
24 799 Evans, D.J.A., Storrar, R.D. & Rea, B.R. (2016). Crevasse-squeeze ridge corridors:  
25 800 Diagnostic features of late-stage palaeo-ice stream activity. *Geomorphology* **258**, 40–  
26 801 50.
- 27  
28 802 Evans, D.J.A. & Twigg, D.R. (2002). The active temperate glacial landsystem: a model  
29 803 based on Breiðamerkurjökull and Fjallsjökull, Iceland. *Quaternary Science Reviews* **21**  
30 804 (20-22), 2143–2177.
- 31  
32 805 Evans, D.J.A., Young, N.J.P. & Ó Cofaigh, C. (2014). Glacial geomorphology of terrestrial-  
33 806 terminating fast flow lobes/ice stream margins in the southwest Laurentide Ice Sheet.  
34 807 *Geomorphology* **204**, 86–113.
- 35  
36 808 Evenson, E.B., Burkhart, P.A., Gosse, J.C., Baker, G.S., Jackofsky, D., Meglioli, A., Dalziel,  
37 809 I., Kraus, S., Alley, R.B. & Berti, C. (2009). Enigmatic boulder trains, supraglacial rock  
38 810 avalanches, and the origin of 'Darwin's boulders,' Tierra del Fuego. *GSA Today* **19** (12),  
39 811 4–10.
- 40  
41 812 Eyles, N. (1979). Facies of supraglacial sedimentation on Icelandic and Alpine temperate  
42 813 glaciers. *Canadian Journal of Earth Sciences* **16** (7), 1341–1361.
- 43  
44 814 Glasser, N. & Jansson, K. (2008). The Glacial Map of southern South America. *Journal of*  
45 815 *Maps* **4** (1), 175–196.
- 46  
47 816 Glasser, N.F. & Jansson, K.N. (2005). Fast-flowing outlet glaciers of the Last Glacial  
48 817 Maximum Patagonian Icefield. *Quaternary Research* **63** (2), 206–211.
- 49  
50 818 Glasser, N.F., Jansson, K.N., Harrison, S. & Kleman, J. (2008). The glacial geomorphology  
51 819 and Pleistocene history of South America between 38 degrees S and 56 degrees S.  
52 820 *Quaternary Science Reviews* **27** (3-4), 365–390.
- 53  
54 821 Glasser, N.F., Jansson, K.N., Harrison, S. & Rivera, A. (2005). Geomorphological evidence  
55 822 for variations of the North Patagonian Icefield during the Holocene. *Geomorphology* **71**  
56 823 (3-4), 263–277.
- 57  
58 824 Hall, B.L., Porter, C.T., Denton, G.H., Lowell, T. V & Bromley, G.R.M. (2013). Extensive  
59 825 recession of Cordillera Darwin glaciers in southernmost South America during Heinrich  
60 826 Stadial 1. *Quaternary Science Reviews* **62** (0), 49–55.
- 827 Ham, N.R. & Attig, J.W. (1996). Ice wastage and landscape evolution along the southern  
828 margin of the Laurentide Ice Sheet, north-central Wisconsin. *Boreas* **25** (3), 171–186.

- 1  
2  
3 829 Harris, C., Williams, G., Brabham, P., Eaton, G. & McCarroll, D. (1997). Glaciotectonized  
4 830 quaternary sediments at Dinas Dinlle, Gwynedd, North Wales, and their bearing on the  
5 831 style of deglaciation in the Eastern Irish Sea. *Quaternary Science Reviews* **16** (1), 109–  
6 832 127.
- 7  
8 833 Hein, A.S., Hulton, N.R.J., Dunai, T.J., Sugden, D.E., Kaplan, M.R. & Xu, S. (2010). The  
9 834 chronology of the Last Glacial Maximum and deglacial events in central Argentine  
10 835 Patagonia. *Quaternary Science Reviews* **29** (9-10), 1212–1227.
- 11 836 Hulton, N.R.J., Purves, R.S., McCulloch, R.D., Sugden, D.E. & Bentley, M.J. (2002). The  
12 837 Last Glacial Maximum and deglaciation in southern South America. *Quaternary*  
13 838 *Science Reviews* **21** (1-3), 233–241.
- 14  
15 839 Johnson, M. & Clayton, L. (2003). Supraglacial landsystems in lowland terrain. In: D. J. A.  
16 840 Evans (ed.). *Glacial Landsystems*. 228–258, London: Hodder Arnold.
- 17  
18 841 Kaplan, M.R., Coronato, A., Hulton, N.R.J., Rabassa, J.O., Kubik, P.W. & Freeman, S.P.H.T.  
19 842 (2007). Cosmogenic nuclide measurements in southernmost South America and  
20 843 implications for landscape change. *Geomorphology* **87** (4), 284–301.
- 21 844 Kaplan, M.R., Fogwill, C.J., Sugden, D.E., Hulton, N., Kubik, P.W. & Freeman, S.P.H.T.  
22 845 (2008a). Southern Patagonian glacial chronology for the Last Glacial period and  
23 846 implications for Southern Ocean climate. *Quaternary Science Reviews* **27** (3-4), 284–  
24 847 294.
- 25  
26 848 Kaplan, M.R., Hein, A.S., Hubbard, A. & Lax, S.M. (2009). Can glacial erosion limit the  
27 849 extent of glaciation? *Geomorphology* **103** (2), 172–179.
- 28  
29 850 Kaplan, M.R., Moreno, P.I. & Rojas, M. (2008b). Glacial dynamics in southernmost South  
30 851 America during Marine Isotope Stage 5e to the Younger Dryas chron: a brief review  
31 852 with a focus on cosmogenic nuclide measurements. *Journal of Quaternary Science* **23**  
32 853 (6-7), 649–658.
- 33 854 Kelley, S.E., Kaplan, M.R., Schaefer, J.M., Andersen, B.G., Barrell, D.J.A., Putnam, A.E.,  
34 855 Denton, G.H., Schwartz, R., Finkel, R.C. & Doughty, A.M. (2014). High-precision <sup>10</sup>Be  
35 856 chronology of moraines in the Southern Alps indicates synchronous cooling in  
36 857 Antarctica and New Zealand 42,000 years ago. *Earth and Planetary Science Letters*  
37 858 **405**, 194–206.
- 38  
39 859 Kilian, R., Baeza, O., Ríos, F., Arz, H., Lamy, F., Witz, J. & Baque, J. (2013). Evolución  
40 860 paleogeográfica y palaeoecológica del Sistema de fiordos del Seno Skyring y Seno  
41 861 Otway en la región de Magallanes durante el tardiglacial y Holoceno. *Anales del*  
42 862 *Instituto de la Patagonia*. [Online]. 41 (2) p.5–26.
- 43 863 Kilian, R. & Lamy, F. (2012). A review of Glacial and Holocene paleoclimate records from  
44 864 southernmost Patagonia (49–55°S). *Quaternary Science Reviews* **53** (0), 1–23.
- 45  
46 865 Kilian, R., Schneider, C., Koch, J., Fesq-Martin, M., Biester, H., Casassa, G., Arévalo, M.,  
47 866 Wendt, G., Baeza, O. & Behrmann, J. (2007). Palaeoecological constraints on late  
48 867 Glacial and Holocene ice retreat in the Southern Andes (53°S). *Global and Planetary*  
49 868 *Change* **59** (1–4), 49–66.
- 50  
51 869 Kjaer, K.H. & Kruger, J. (2001). The final phase of dead-ice moraine development:  
52 870 processes and sediment architecture, Kotlujokull, Iceland. *Sedimentology* **48** (5), 935–  
53 871 952.
- 54 872 Kleman, J., Hättestrand, C., Stroeven, A.P., Jansson, K., De Angelis, H. & Borgström, I.  
55 873 (2006). Reconstruction of palaeo-ice sheets - inversion of their glacial  
56 874 geomorphological record. In: P. Knight (ed.). *Glaciology and Earth's Changing*  
57 875 *Environment*. 192–198, Blackwell.

- 1  
2  
3 876 Krüger, J. (1994). Glacial processes, sediments, landforms and stratigraphy in the terminus  
4 877 region of Myrdalsjökull, Iceland. *Folia Geographica Danica* **21**, 1–233.
- 5  
6 878 Lamy, F., Kaiser, J., Arz, H.W., Hebbeln, D., Ninnemann, U., Timm, O., Timmermann, A. &  
7 879 Toggweiler, J.R. (2007). Modulation of the bipolar seesaw in the Southeast Pacific  
8 880 during Termination 1. *Earth and Planetary Science Letters* **259** (3–4), 400–413.
- 9  
10 881 Lovell, H., Fleming, E.J., Benn, D.I., Hubbard, B., Lukas, S., Rea, B.R., Noormets, R. &  
11 882 Flink, A.E. (2015). Debris entrainment and landform genesis during tidewater glacier  
12 883 surges. *Journal of Geophysical Research: Earth Surface* **120** (8), 1574–1595.
- 13  
14 884 Lovell, H., Stokes, C.R. & Bentley, M.J. (2011). A glacial geomorphological map of the Seno  
15 885 Skyring-Seno Otway-Strait of Magellan region, southernmost Patagonia. *Journal of*  
16 886 *Maps* **7** (1), 318–339.
- 17  
18 887 Lovell, H., Stokes, C.R., Bentley, M.J. & Benn, D.I. (2012). Evidence for rapid ice flow and  
19 888 proglacial lake evolution around the central Strait of Magellan region, southernmost  
20 889 Patagonia. *Journal of Quaternary Science* **27** (6), 625–638.
- 21  
22 890 McCulloch, R.D. & Bentley, M.J. (1998). Late glacial ice advances in the Strait of Magellan,  
23 891 southern Chile. *Quaternary Science Reviews* **17** (8), 775–787.
- 24  
25 892 McCulloch, R.D., Bentley, M.J., Tipping, R.M. & Clapperton, C.M. (2005a). Evidence for late-  
26 893 glacial ice dammed lakes in the central Strait of Magellan and Bahia Inutil,  
27 894 southernmost South America. *Geografiska Annaler Series a-Physical Geography* **87A**  
28 895 (2), 335–362.
- 29  
30 896 McCulloch, R.D., Fogwill, C.J., Sugden, D.E., Bentley, M.J. & Kubik, P.W. (2005b).  
31 897 Chronology of the last glaciation in central Strait of Magellan and Bahia Inutil,  
32 898 southernmost South America. *Geografiska Annaler Series a-Physical Geography* **87A**  
33 899 (2), 289–312.
- 34  
35 900 Meglioli, A. (1992). *Glacial Geology and Chronology of southernmost Patagonia and Tierra*  
36 901 *del Fuego, Argentina and Chile*. Lehigh University.
- 37  
38 902 Mercer, J.H. (1976). Glacial history of southernmost South America. *Quaternary Research* **6**  
39 903 (2), 125–166.
- 40  
41 904 Oldale, R.N. & O'Hara, C.J. (1984). Glaciotectonic origin of the Massachusetts coastal end  
42 905 moraines and a fluctuating late Wisconsinan ice margin. *Geological Society of America*  
43 906 *Bulletin* **95** (1), 61–74.
- 44  
45 907 Peltier, W.R. (2004). Global glacial isostasy and the surface of the ice-age earth: The ICE-  
46 908 5G (VM2) Model and GRACE. *Annual Review of Earth and Planetary Sciences* **32** (1),  
47 909 111–149.
- 48  
49 910 Phillips, E., Lee, J.R. & Burke, H. (2008a). Progressive proglacial to subglacial deformation  
50 911 and syntectonic sedimentation at the margins of the Mid-Pleistocene British Ice Sheet:  
51 912 evidence from north Norfolk, UK. *Quaternary Science Reviews* **27** (19–20), 1848–1871.
- 52  
53 913 Phillips, E., Evans, D.J. & Auton, C. (2002). Polyphase deformation at an oscillating ice  
54 914 margin following the Loch Lomond Readvance, central Scotland, UK. *Sedimentary*  
55 915 *Geology* **149** (1–3), 157–182.
- 56  
57 916 Phillips, W.M., Hall, A.M., Ballantyne, C.K., Binnie, S., Kubik, P.W. & Freeman, S. (2008b).  
58 917 Extent of the last ice sheet in northern Scotland tested with cosmogenic <sup>10</sup>Be exposure  
59 918 ages. *Journal of Quaternary Science* **23** (2), 101–107.
- 60  
61 919 Porter, S., Clapperton, C. & Sugden, D. (1992). Chronology and dynamics of deglaciation  
62 920 along and near the Strait of Magellan, southernmost South America. *SGU series Ca.*  
63 921 *Research paper*

- 1  
2  
3 922 Porter, S.C. (1990). Character and ages of Pleistocene Drifts in a transect across the Strait  
4 923 of Magellan. *Quaternary of South America and Antarctica Peninsula* **7**, 35–49.
- 5  
6 924 Price, R. (1970). Moraines at Fjallsjökull, Iceland. *Arctic and Alpine Research* **2**, 27–42.
- 7 925 Putnam, A.E., Schaefer, J.M., Denton, G.H., Barrell, D.J.A., Birkel, S.D., Andersen, B.G.,  
8 926 Kaplan, M.R., Finkel, R.C., Schwartz, R. & Doughty, A.M. (2013). The Last Glacial  
9 927 Maximum at 44°S documented by a <sup>10</sup>Be moraine chronology at Lake Ohau, Southern  
10 928 Alps of New Zealand. *Quaternary Science Reviews* **62**, 114–141.
- 11 929 Rabassa, J. (2008). Late Cenozoic Glaciations in Patagonia and Tierra del Fuego. In: J.  
12 930 Rabassa (ed.). *Developments in Quaternary Sciences*. **11**, 151–204, Elsevier.
- 13  
14 931 Rabassa, J., Coronato, A., Bujalesky, G., Salemme, M., Roig, C., Meglioli, A., Heusser, C.,  
15 932 Gordillo, S., Roig, F., Borrromei, A. & Quattrocchio, M. (2000). Quaternary of Tierra del  
16 933 Fuego, Southernmost South America: an updated review. *Quaternary International* **68-**  
17 934 **71** (0), 217–240.
- 18  
19 935 Raedecke, L.D. (1978). Formas del terreno y depositos cuaternarios Tierra del Fuego  
20 936 central, Chile. *Revista geológica de Chile* **5**, 3–31.
- 21  
22 937 Rotnicki, K. (1976). The theoretical basis for and a model of the origin of glaciotectionic  
23 938 deformations. *Quaestiones Geographicae* **3**, 103–139.
- 24  
25 939 Rutter, N., Schnack, E.J., Rio, J. del, Fasano, J.L., Isla, F.I. & Radtke, U. (1989). Correlation  
26 940 and dating of Quaternary littoral zones along the Patagonian coast, Argentina.  
27 941 *Quaternary Science Reviews* **8** (3), 213–234.
- 28 942 Sagredo, E.A., Moreno, P.I., Villa-Martinez, R., Kaplan, M.R., Kubik, P.W. & Stern, C.R.  
29 943 (2011). Fluctuations of the Última Esperanza ice lobe (52°S), Chilean Patagonia, during  
30 944 the last glacial maximum and termination 1. *Geomorphology* **125** (1), 92–108.
- 31 945 Schaefer, J.M., Putnam, A.E., Denton, G.H., Kaplan, M.R., Birkel, S., Doughty, A.M., Kelley,  
32 946 S., Barrell, D.J.A.A., Finkel, R.C., Winckler, G., Anderson, R.F., Ninneman, U.S.,  
33 947 Barker, S., Schwartz, R., Andersen, B.G. & Schluechter, C. (2015). The Southern  
34 948 Glacial Maximum 65,000 years ago and its Unfinished Termination. *Quaternary*  
35 949 *Science Reviews* **114**, 52–60.
- 36  
37 950 Schomacker, A. (2008). What controls dead-ice melting under different climate conditions? A  
38 951 discussion. *Earth-Science Reviews* **90** (3–4), 103–113.
- 39  
40 952 Schomacker, A., Benediktsson, Í.Ö. & Ingólfsson, Ó. (2014). The Eyjabakkajökull glacial  
41 953 landsystem, Iceland: Geomorphic impact of multiple surges. *Geomorphology* **218**, 98–  
42 954 107.
- 43 955 Sharp, M. (1985). ‘Crevasse-Fill’ Ridges: A Landform Type Characteristic of Surging  
44 956 Glaciers? *Geografiska Annaler, Series A: Physical Geography* **67** (3/4), 213–220.
- 45  
46 957 Singer, B.S., Ackert, R.P. & Guillou, H. (2004). <sup>40</sup>Ar/<sup>39</sup>Ar and K-Ar chronology of  
47 958 Pleistocene glaciations in Patagonia. *Geological Society of America Bulletin* **116** (3-4),  
48 959 434–450.
- 49  
50 960 Spedding, N. & Evans, D.J.. (2002). Sediments and landforms at Kvíárjökull, southeast  
51 961 Iceland: a reappraisal of the glaciated valley landsystem. *Sedimentary Geology* **149** (1-  
52 962 3), 21–42.
- 53 963 Stern, C.R., Moreno, P.I., Villa-Martínez, R., Sagredo, E.A., Prieto, A. & Labarca, R. (2011).  
54 964 Evolution of ice-dammed proglacial lakes in Última Esperanza, Chile: implications from  
55 965 the late-glacial R1 eruption of Reclús volcano, Andean Austral Volcanic Zone. *Andean*  
56 966 *geology* **38**, 82–97.
- 57  
58 967 Stokes, C.R. & Clark, C.D. (2004). Evolution of late glacial ice-marginal lakes on the  
59  
60

- 1  
2  
3 968 northwestern Canadian Shield and their influence on the location of the Dubawnt Lake  
4 969 palaeo-ice stream. *Palaeogeography, Palaeoclimatology, Palaeoecology* **215** (1-2),  
5 970 155–171.
- 6  
7 971 Stokes, C.R. & Clark, C.D. (1999). Geomorphological criteria for identifying Pleistocene ice  
8 972 streams. *Annals of Glaciology* **28** (1), 67–74.
- 9  
10 973 Stokes, C.R. & Clark, C.D. (2001). Palaeo-ice streams. *Quaternary Science Reviews* **20**  
11 974 (13), 1437–1457.
- 12  
13 975 Stokes, C.R., Spagnolo, M. & Clark, C.D. (2011). The composition and internal structure of  
14 976 drumlins: Complexity, commonality, and implications for a unifying theory of their  
15 977 formation. *Earth-Science Reviews* **107** (3-4), 398–422.
- 16  
17 978 Storrar, R.D., Stokes, C.R. & Evans, D.J.A. (2014a). Increased channelization of subglacial  
18 979 drainage during deglaciation of the Laurentide Ice Sheet. *Geology* **42** (3), 239–242.
- 19  
20 980 Storrar, R.D., Stokes, C.R. & Evans, D.J.A. (2014b). Morphometry and pattern of a large  
21 981 sample (>20,000) of Canadian eskers and implications for subglacial drainage beneath  
22 982 ice sheets. *Quaternary Science Reviews* **105**, 1–25.
- 23  
24 983 Sugden, D.E., Bentley, M.J., Fogwill, C.J., Hulton, N.R.J., McCulloch, R.D. & Purves, R.S.  
25 984 (2005). Late-glacial glacier events in southernmost South America: A blend of  
26 985 'northern' and 'southern' hemispheric climatic signals? *Geografiska Annaler Series a-*  
27 986 *Physical Geography* **87A** (2), 273–288.
- 28  
29 987 Teller, J.T. (2003). Subaquatic landsystems: large proglacial lakes. In: D. J. A. Evans (ed.).  
30 988 *Glacial Landsystems*. 348–371, London: Hodder Arnold.
- 31  
32 989 van der Wateren, F. (1995). Structural geology and sedimentology of push moraines:  
33 990 processes of soft sediment deformation in a glacial environment and the distribution of.  
34 991 *Mededelingen Rijks Geologische Dienst* **54**.
- 35  
36 992 Williams, G.D., Brabham, P.J., Eaton, G.P. & Harris, C. (2001). Late Devensian  
37 993 glaciotectonic deformation at St Bees, Cumbria: a critical wedge model. *Journal of the*  
38 994 *Geological Society* **158** (1), 125–135.
- 39  
40  
41  
42  
43  
44  
45  
46  
47  
48  
49  
50  
51  
52  
53  
54  
55  
56  
57  
58  
59  
60

996 **10 Figure captions**

997 Figure 1. (A) Location of the study area in southern South America. (B) Overview of the  
998 geomorphological map from Darvill et al. (2014) showing the locations of figures and  
999 locations mentioned in the text. (C) Stylised representation of the southernmost part of the  
1000 former Patagonian Ice Sheet, highlighting the five former ice lobes discussed in this paper.  
1001 The approximate position of the ice divide is based on Hulton et al. (2002), but is shown for  
1002 illustrative purposes only.

1003 Figure 2. An overview of the glacial geomorphology relating to the Río Gallegos, Skyring,  
1004 Otway and Magellan lobes, including key locations mentioned in the text (location shown in  
1005 Figure 1).

1006 Figure 3. (A) Overview of the glacial geomorphology associated with the centre of the BI-  
1007 SSb lobe (location shown in Figure 1). Note the spillway marked by former shorelines  
1008 associated with a proglacial lake that drained at Onaisín through Laguna Larga. (B)  
1009 Enlargement of the central part of (A) showing cross-cutting relationships between subdued  
1010 moraine topography and moraine ridges, glacial lineations and smaller hummocky terrain.  
1011 (C) Enlargement of (B) showing the ordered nature of the regular hummocky terrain mini-  
1012 ridges and the cross-cutting relationships more clearly.

1013 Figure 4. (A) Overview of the glacial geomorphology associated with the Magellan lobe  
1014 (location shown in Figure 1). Península Juan Mazía may have been the terminus of a surge-  
1015 like advance (see text). (B) Enlargement of Punta Gente and the large field of elongate  
1016 drumlins, in places draped by small moraine ridges.

1017 Figure 5. Sketch log (A) and accompanying photographs (B and C) of proglacially tectonised  
1018 lacustrine silts and sands within an end moraine of the BI-SSb lobe (location shown in Figure  
1019 3A). There is a high degree of folding and faulting. The large section suggests that the ice  
1020 lobe retreated sufficiently for a sizeable proglacial lake to develop, prior to re-advance.

1021 Figure 6. Sketch log (A) and accompanying photographs (B and C) of a glaciectonised  
1022 moraine associated with re-advance of the Otway lobe (location shown in Figure 2). The  
1023 normal thrust faults are particularly highlighted by a deformed tephra layer in (C). The  
1024 sediments are characteristic of outwash material that was likely deposited during retreat of  
1025 the ice prior to re-advance and proglacial thrusting.

1026 Figure 7. (A) A Google Earth image of larger irregular hummocky terrain from the south side  
1027 of the BI-SSb lobe. (B) Field photograph of the hummocky topography on the north side of  
1028 the BI-SSb lobe, illustrating the rounded hills and lakes. (C) A section through the inner band  
1029 of larger hummocky terrain on the north side of the BI-SSb lobe. The top unit relates to this  
1030 inner glacial limit (the San Sebastián drift), but overlies an earlier diamict unit and associated  
1031 outwash (the Río Cullen drift), indicating that the ice lobe re-advanced (person for scale).

1032 Figure 8. (A) A Google Earth image of regular hummocky terrain from the centre of the BI-  
1033 SSb lobe (location shown in Figure 3B). This terrain resembles geometrical ridge networks  
1034 and could be preserved crevasse-squeeze ridges. To illustrate this, (B) shows a Microsoft  
1035 Bing Maps image of crevasse-squeeze ridges in front of the surging Brúarjökull glacier in

1  
2  
3 1036 Iceland. Note that although the glaciers in question are markedly different in size, the images  
4 1037 are at the same scale.

5  
6 1038 Figure 9. Glacial geomorphology found at the intersection between the Río Gallegos and  
7 1039 Skyring lobes (location shown in Figure 2). (1) to (4) show a stylised formation mechanism  
8 1040 for the irregular dissected ridge features. (1) The Río Gallegos advances first, creating a  
9 1041 swath of drumlins (2), and possibly moraines, that are later overridden by an advance of the  
10 1042 Skyring lobe (3). The order is dictated by the flow of meltwater from the Skyring lobe into the  
11 1043 Río Gallegos basin (4).

12  
13  
14 1044 Figure 10. Evidence for proglacial lakes within the study area. (A) shows the geomorphology  
15 1045 and (B) the reconstructed ice limit and palaeo-Laguna Blanca proglacial lake just prior to  
16 1046 drainage, when discharge flowed northwards. (C) The geomorphological evidence for lake  
17 1047 drainage eastward into the Strait of Magellan once the Skyring lobe retreated beyond the  
18 1048 bluff separating it from the Otway lobe (locations shown in Figure 2). (D) Raised shorelines,  
19 1049 (E) laminated lake sediments with a dropstone circled, and (F) a drainage channel  
20 1050 associated with palaeo-Laguna Blanca (locations shown in A and B). (G) Rhythmically  
21 1051 laminated sediments from Laguna Verde (see Figure 4 for location). (H) Enlarged part of (G)  
22 1052 showing several heavily deformed layers, possibly due to earthquake-induced tectonisation.  
23 1053 (I) Dropstones are found within the Laguna Verde sequence (circled).

24  
25  
26 1054 Figure 11. Glacial geomorphology of (A) the BI-SSb lobe and (B) the Río Gallegos, Skyring,  
27 1055 Otway and Magellan lobes. The geomorphology has been grouped and re-coloured  
28 1056 according to the three dominant landform suites indicative of an active temperate glacial  
29 1057 landsystem.

30  
31  
32 1058 Figure 12. (A) Simplified version of the glacial geomorphology in the study area to show the  
33 1059 dominant ice flow and ice marginal features. (B) The flow-sets defined in this study (FS 1-  
34 1060 20). (C) The dominant limits associated with four different sets of ice-marginal features.  
35 1061 These were synthesised into glacial limits, shown in (D). The two innermost limits of the  
36 1062 Skyring lobe are from Kilian et al. (2007). Eight of these limits are used in our glacial  
37 1063 reconstruction time steps, coloured according to Figure 14.

38  
39  
40 1064 Figure 13. Reconstructed glacial history for the five ice lobes studied, with eight time steps  
41 1065 shown in (A) to (H). The hypothesised ice divide based on Hulton et al. (2002) is shown in  
42 1066 (A) and (B) for reference. We show the rest of the ice sheet for completeness, with  
43 1067 hypothesised gLGM limits based on Coronato et al. (2004). The rest of the ice sheet would  
44 1068 have retreated over time, but that was not part of our study. Also shown in (A) and (B) are  
45 1069 hypothesised drainage divides between the five ice lobes (bold dashed black lines) and the  
46 1070 lines of topographic profiles for each ice lobe shown in Figure 14 (fine dashed black lines).  
47 1071 Key flow-sets are shown and blue arrows show the direction of lake drainage routes.  
48 1072 Question marks show where the ice configuration is unknown and black arrows in (H) show  
49 1073 final retreat during time step 8. Published chronological data are shown where appropriate  
50 1074 (see text for discussion). These are: argon dates (red text/circles); cosmogenic nuclide  
51 1075 exposure dates (yellow circles) consisting of recalibrated  $^{10}\text{Be}$  dates (black text), recalibrated  
52 1076  $^{26}\text{Al}$  dates (italic blue text) and  $^{36}\text{Cl}$  dates (italic green text); and cosmogenic nuclide depth  
53 1077 profiles (bold black text/circles).

1  
2  
3 1078 Figure 14. Topographic profiles for each ice lobe, shown as changes in elevation relating to  
4 1079 present-day sea-level against distance from the hypothesised ice sheet divide. Ice flowed  
5 1080 from left to right. The profiles from the ice divide to the outermost time step are shown in  
6 1081 Figure 13A and B. The coloured numbers relate to the time steps shown in Figure 13D.  
7 1082 Present-day sea-level is shown (short dashes), as well as the approximate sea-level at the  
8 1083 gLGM (long dashes). Hence, the outermost limits of the BI-SSb lobe were in the Atlantic  
9 1084 Ocean but would have formed on the exposed continental shelf. Also shown are the  
10 1085 approximate heights of former proglacial lakes. The Río Gallegos lake would have dropped  
11 1086 progressively over time, but the timing is not well constrained.

14 1087 Figure 15. A distance-time graph for the five ice lobes over the last glacial cycle, based on  
15 1088 cosmogenic nuclide and radiocarbon dating discussed in the text. Dated lava flows suggest  
16 1089 that most of the ice lobes would have advanced during earlier glacial cycles (Meglioli, 1992;  
17 1090 Singer et al., 2004; Kaplan et al., 2007). The BI-SSb lobe contains a large number of dates,  
18 1091 but with scattered ages and large associated errors. It is not possible to reconcile the  
19 1092 cosmogenic nuclide ages and some of the radiocarbon dates during deglaciation. The  
20 1093 Magellan lobe contains fewer dates, but a more consistent ice-retreat history. The Otway  
21 1094 and Skyring lobes contain few dates, but must have been retreating from a limit prior to *ca.*  
22 1095 30 ka because of the lake drainage from palaeo-Laguna Blanca in front of the Skyring,  
23 1096 Otway and Magellan lobes (the blue stratigraphic correlation bar). Note the similarities in the  
24 1097 glacial histories of these four ice lobes, including retreating from extensive positions prior to  
25 1098 30 ka and the gLGM, and rapid late-stage retreat. The timing of advance and retreat of the  
26 1099 Río Gallegos lobe is not well constrained, partly because many of the cosmogenic nuclide  
27 1100 and radiocarbon dates are from lateral positions that cannot be robustly linked to the former  
28 1101 ice terminus. A large number of radiocarbon dates are shown from (Sagredo et al., 2011),  
29 1102 but these cannot be tied to the ice terminus and are simply shown against the approximate  
30 1103 ice distance in time step 7.

35 1104 Table S1. Compilation of  $^{10}\text{Be}$  and  $^{26}\text{Al}$  cosmogenic nuclide exposure ages from the study  
36 1105 area. Ages have been recalculated.

38 1106 Table S2. Compilation of  $^{36}\text{Cl}$  cosmogenic nuclide exposure ages from the study area. Ages  
39 1107 have not been recalculated.

41 1108 Table S3. Ages from two depth profiles through outwash associated with glacial limits in the  
42 1109 study area. Ages are taken directly from Darvill et al. (2015b).

44 1110 Table S4. Compilation of radiocarbon dates relating to glacier activity within the study area.  
45 1111 Ages have been recalculated.

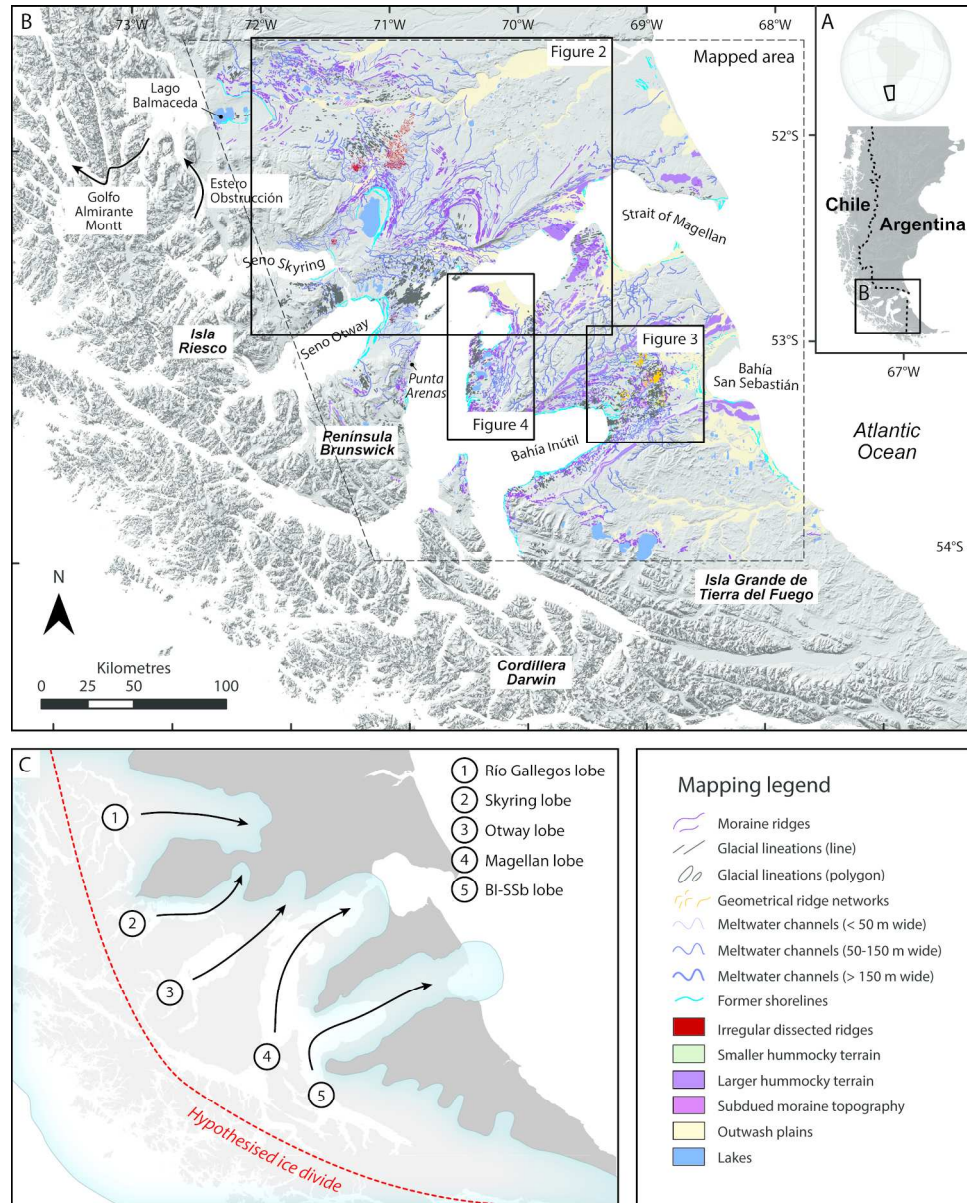
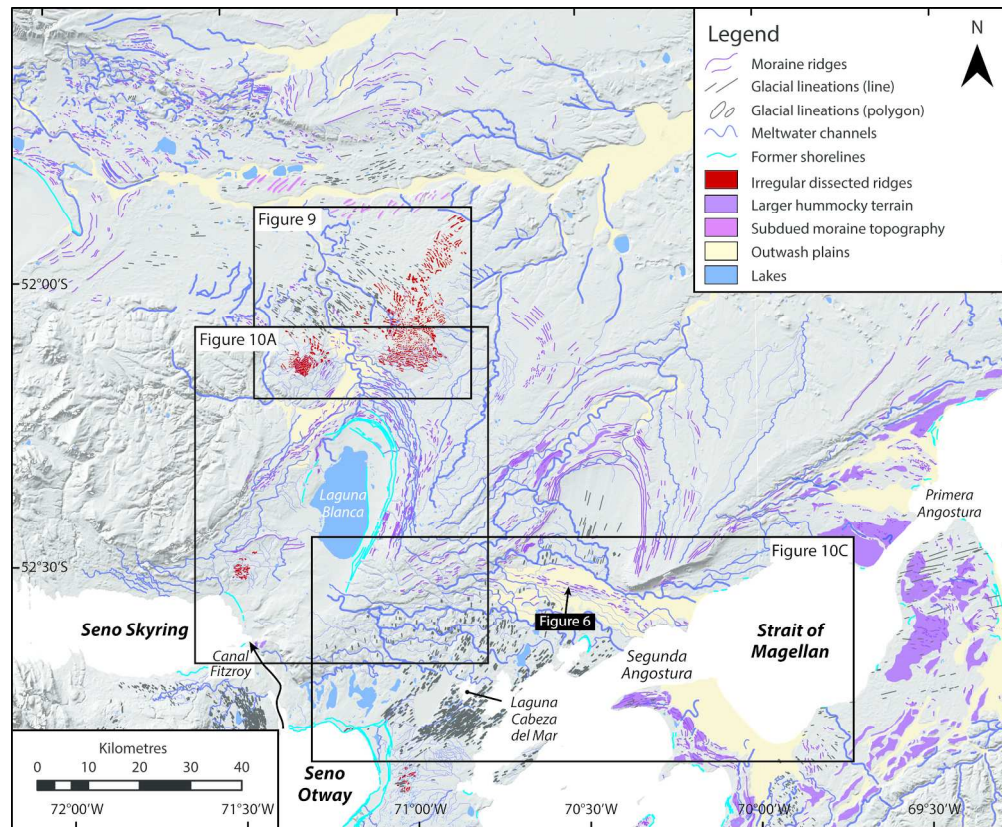


Figure 1. (A) Location of the study area in southern South America. (B) Overview of the geomorphological map from Darvill et al. (2014) showing the locations of figures and locations mentioned in the text. (C) Stylised representation of the southernmost part of the former Patagonian Ice Sheet, highlighting the five former ice lobes discussed in this paper. The approximate position of the ice divide is based on Hulton et al. (2002), but is shown for illustrative purposes only.  
183x228mm (300 x 300 DPI)



34  
35  
36  
37  
38  
39  
40  
41  
42  
43  
44  
45  
46  
47  
48  
49  
50  
51  
52  
53  
54  
55  
56  
57  
58  
59  
60

Figure 2. An overview of the glacial geomorphology relating to the Río Gallegos, Skyring, Otway and Magellan lobes, including key locations mentioned in the text (location shown in Figure 1).  
184x151mm (300 x 300 DPI)

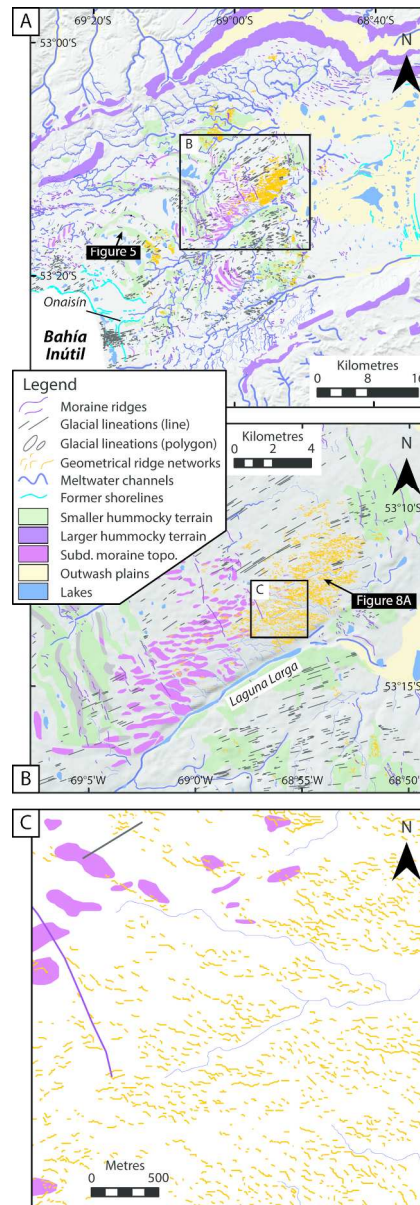


Figure 3. (A) Overview of the glacial geomorphology associated with the centre of the BI-SSb lobe (location shown in Figure 1). Note the spillway marked by former shorelines associated with a proglacial lake that drained at Onaisin through Laguna Larga. (B) Enlargement of the central part of (A) showing cross-cutting relationships between subdued moraine topography and moraine ridges, glacial lineations and smaller hummocky terrain. (C) Enlargement of (B) showing the ordered nature of the regular hummocky terrain mini-ridges and the cross-cutting relationships more clearly.  
85x245mm (300 x 300 DPI)

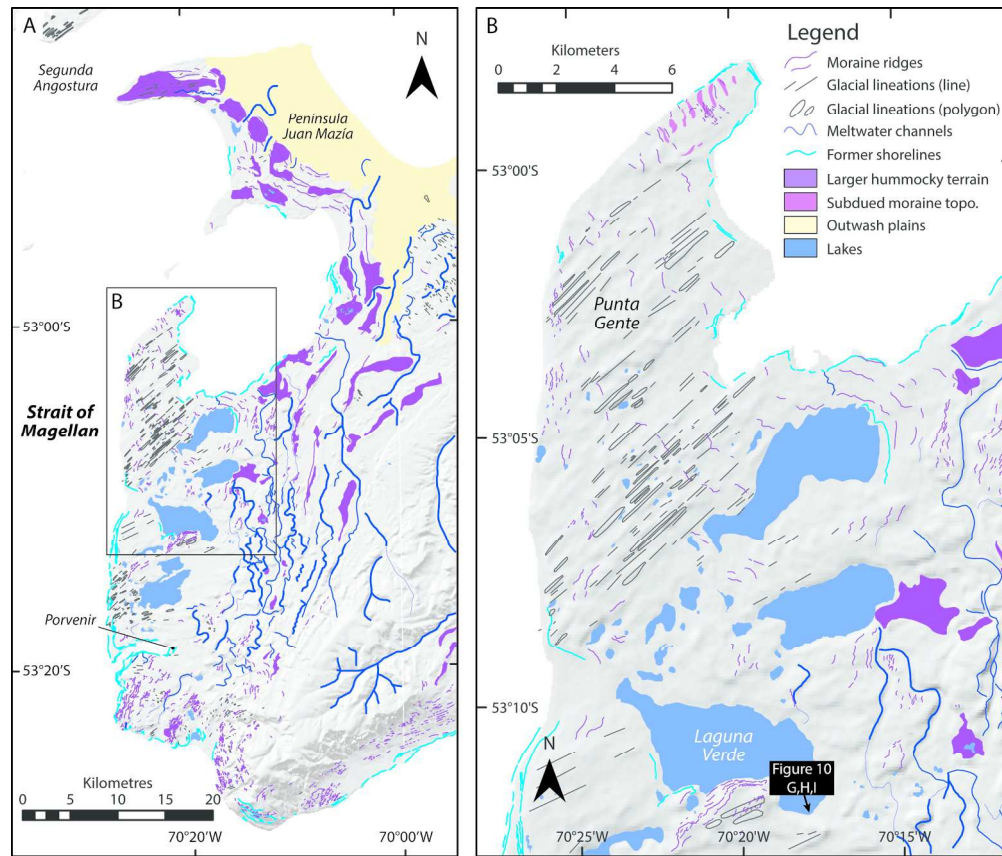


Figure 4. (A) Overview of the glacial geomorphology associated with the Magellan lobe (location shown in Figure 1). Península Juan Mazía may have been the terminus of a surge-like advance (see text). (B) Enlargement of Punta Gente and the large field of elongate drumlins, in places draped by small moraine ridges.

183x156mm (300 x 300 DPI)

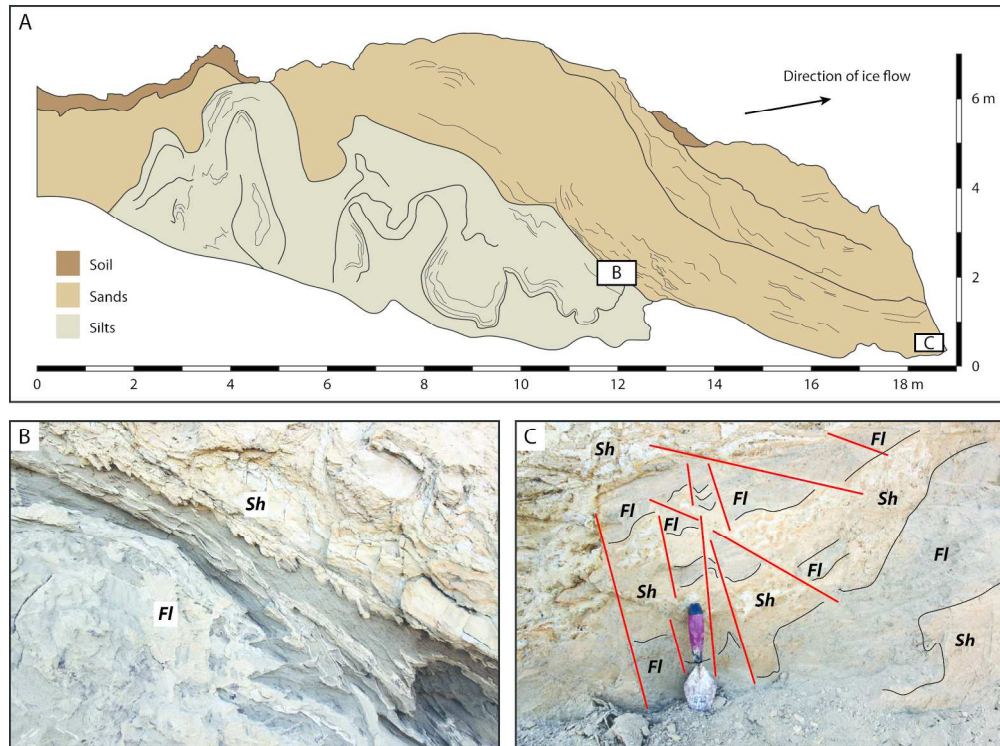


Figure 5. Sketch log (A) and accompanying photographs (B and C) of proglacially tectonised lacustrine silts and sands within an end moraine of the BI-SSb lobe (location shown in Figure 3A). There is a high degree of folding and faulting. The large section suggests that the ice lobe retreated sufficiently for a sizeable proglacial lake to develop, prior to re-advance.

183x136mm (300 x 300 DPI)

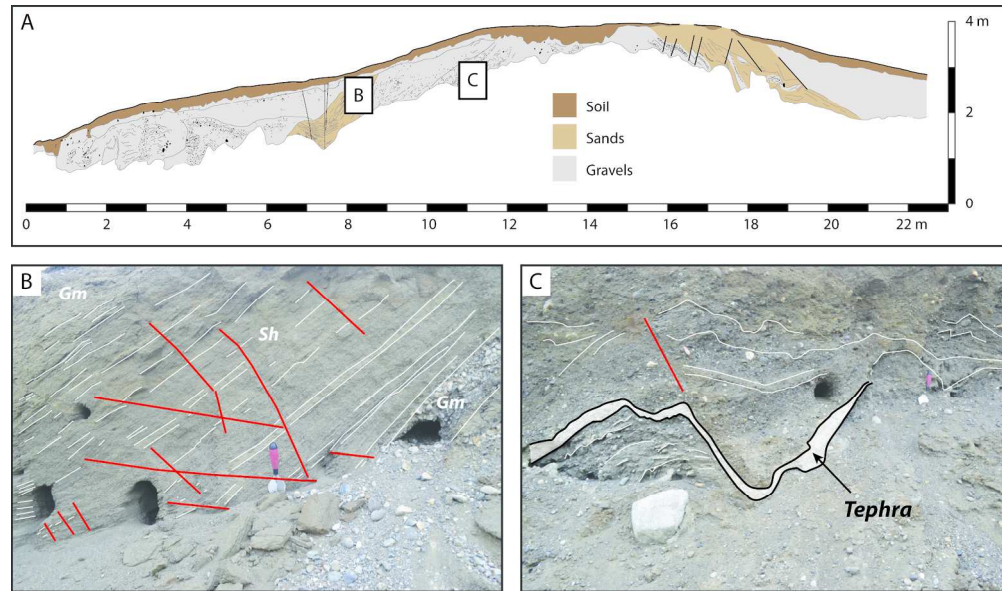


Figure 6. Sketch log (A) and accompanying photographs (B and C) of a glaciotectionised moraine associated with re-advance of the Otway lobe (location shown in Figure 2). The normal thrust faults are particularly highlighted by a deformed tephra layer in (C). The sediments are characteristic of outwash material that was likely deposited during retreat of the ice prior to re-advance and proglacial thrusting.  
183x108mm (300 x 300 DPI)

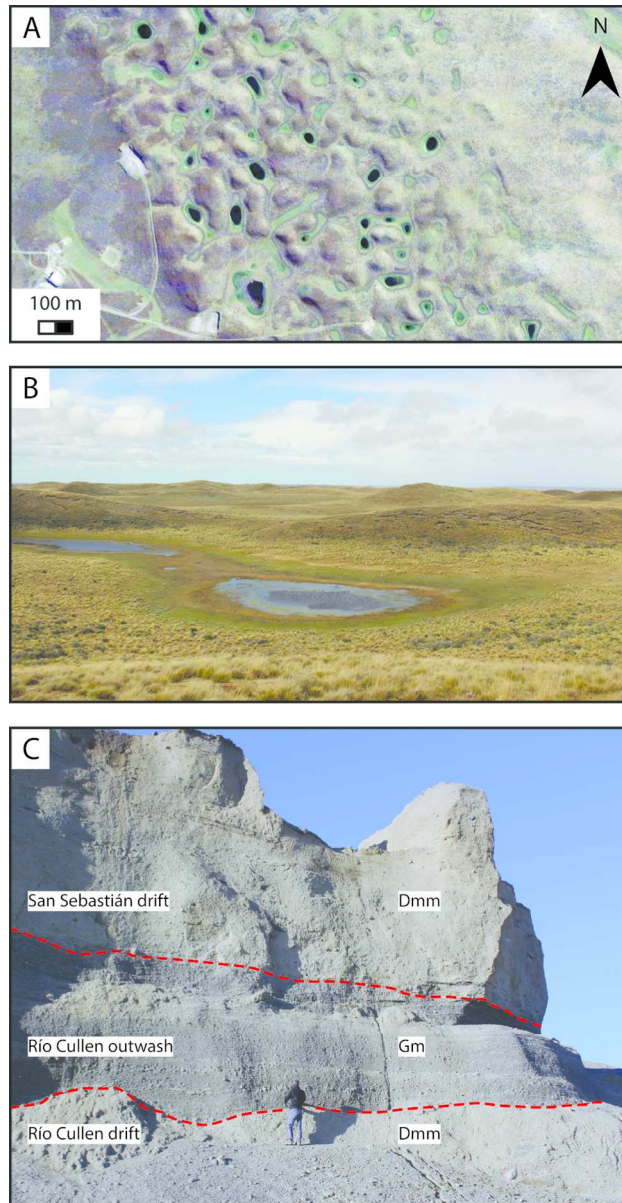


Figure 7. (A) A Google Earth image of larger irregular hummocky terrain from the south side of the BI-SSb lobe. (B) Field photograph of the hummocky topography on the north side of the BI-SSb lobe, illustrating the rounded hills and lakes. (C) A section through the inner band of larger hummocky terrain on the north side of the BI-SSb lobe. The top unit relates to this inner glacial limit (the San Sebastián drift), but overlies an earlier diamict unit and associated outwash (the Río Cullen drift), indicating that the ice lobe re-advanced (person for scale).

85x164mm (300 x 300 DPI)

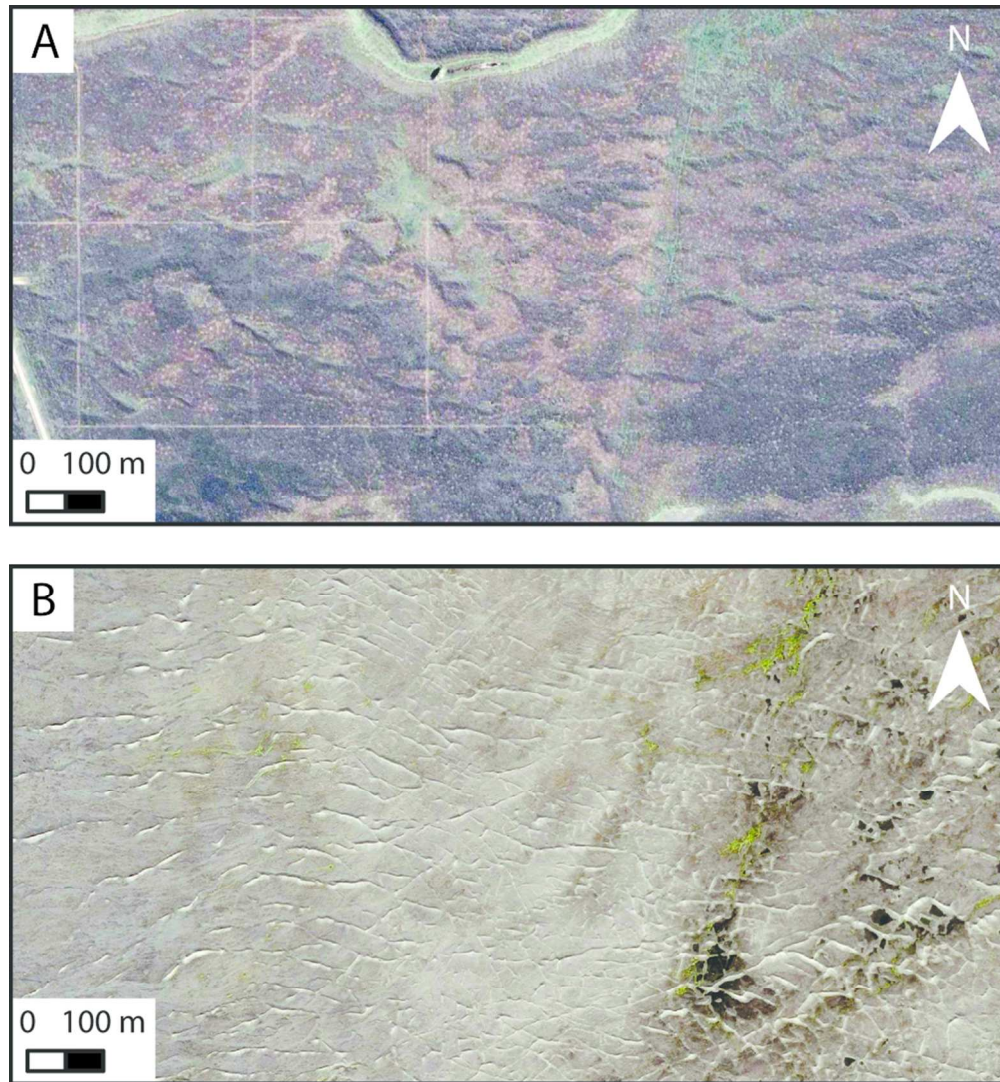


Figure 8. (A) A Google Earth image of regular hummocky terrain from the centre of the BI-SSb lobe (location shown in Figure 3B). This terrain resembles geometrical ridge networks and could be preserved crevasse-squeeze ridges. To illustrate this, (B) shows a Microsoft Bing Maps image of crevasse-squeeze ridges in front of the surging Brúarjökull glacier in Iceland. Note that although the glaciers in question are markedly different in size, the images are at the same scale.  
85x92mm (300 x 300 DPI)

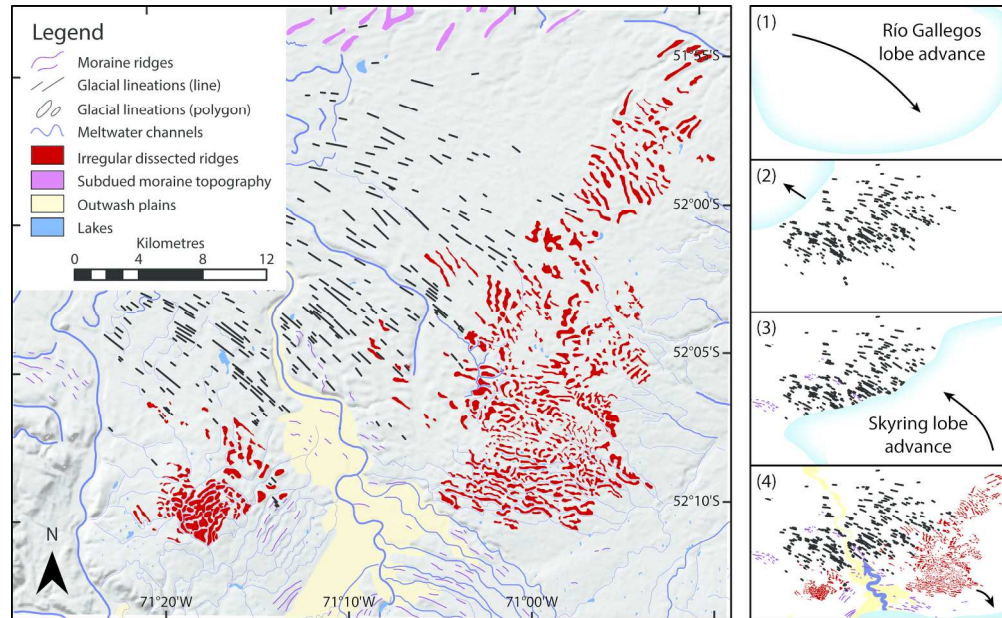


Figure 9. Glacial geomorphology found at the intersection between the Río Gallegos and Skyring lobes (location shown in Figure 2). (1) to (4) show a stylised formation mechanism for the irregular dissected ridge features. (1) The Río Gallegos advances first, creating a swath of drumlins (2), and possibly moraines, that are later overridden by an advance of the Skyring lobe (3). The order is dictated by the flow of meltwater from the Skyring lobe into the Río Gallegos basin (4).  
183x112mm (300 x 300 DPI)

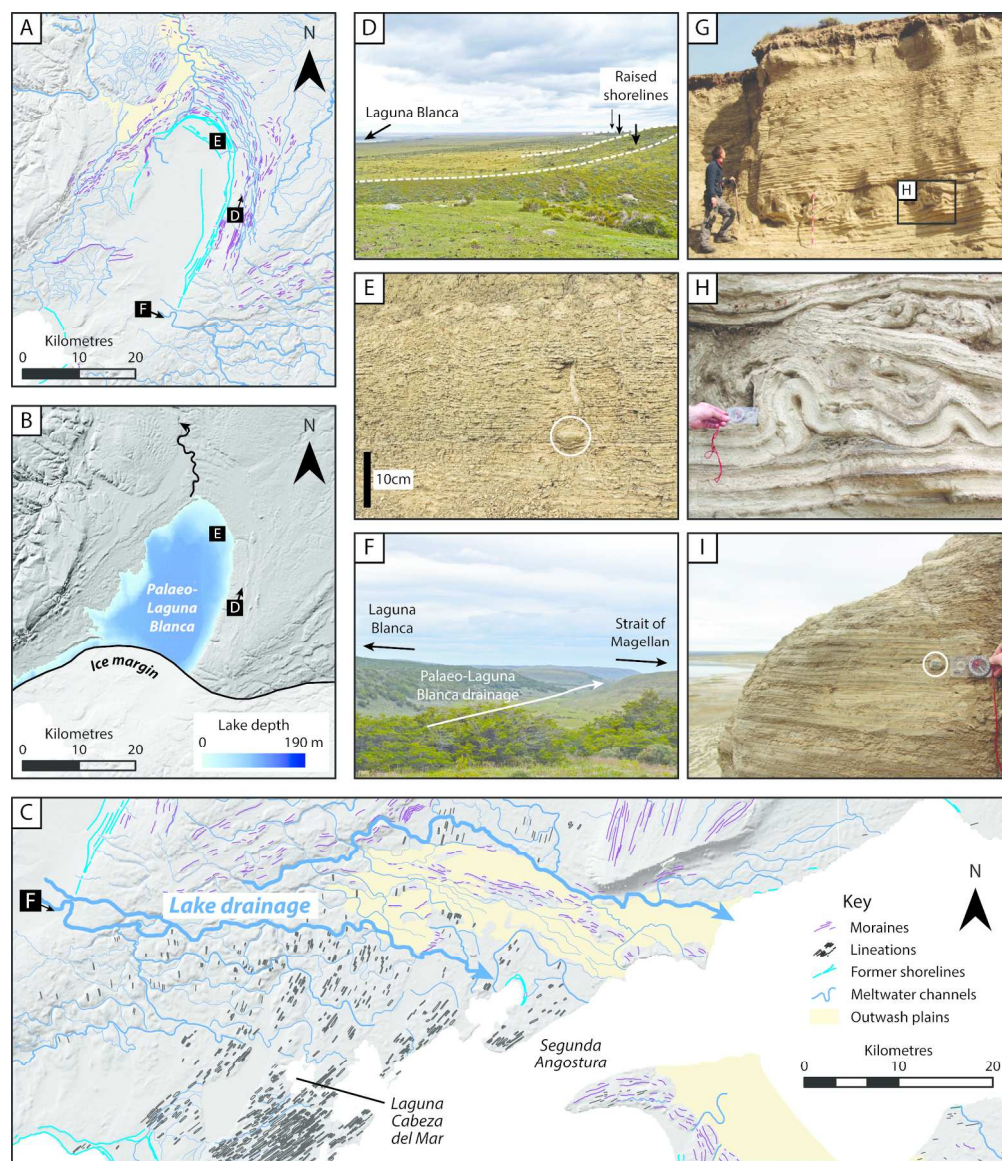


Figure 10. Evidence for proglacial lakes within the study area. (A) shows the geomorphology and (B) the reconstructed ice limit and palaeo-Laguna Blanca proglacial lake just prior to drainage, when discharge flowed northwards. (C) The geomorphological evidence for lake drainage eastward into the Strait of Magellan once the Skyring lobe retreated beyond the bluff separating it from the Otway lobe (locations shown in Figure 2). (D) Raised shorelines, (E) laminated lake sediments with a dropstone circled, and (F) a drainage channel associated with palaeo-Laguna Blanca (locations shown in A and B). (G) Rhythmically laminated sediments from Laguna Verde (see Figure 4 for location). (H) Enlarged part of (G) showing several heavily deformed layers, possibly due to earthquake-induced tectonisation. (I) Dropstones are found within the Laguna Verde sequence (circled).

183x212mm (300 x 300 DPI)

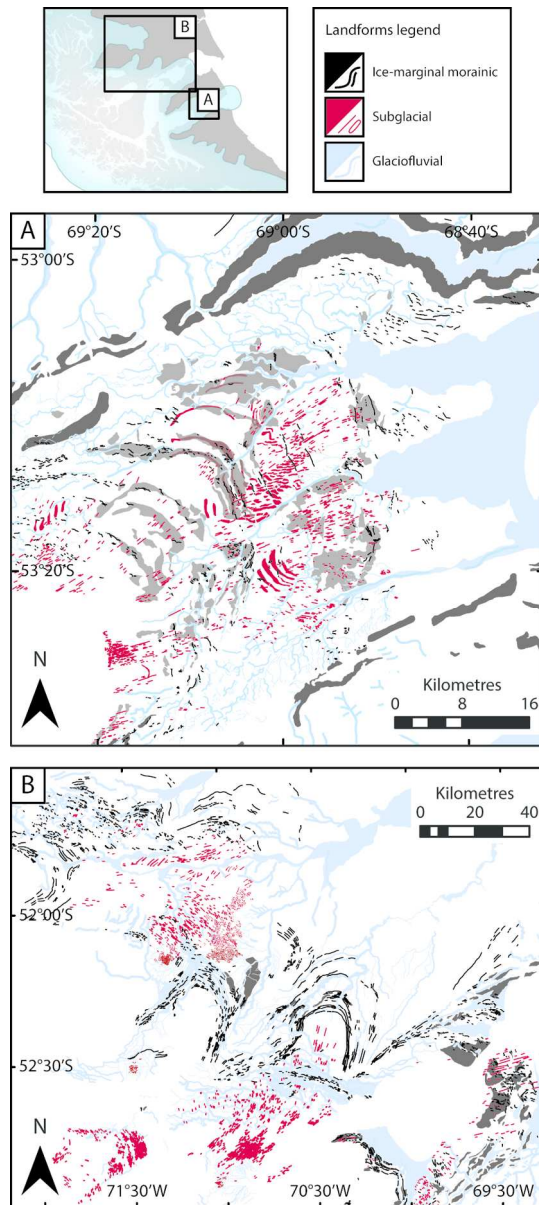


Figure 11. Glacial geomorphology of (A) the BI-SSb lobe and (B) the Río Gallegos, Skyring, Otway and Magellan lobes. The geomorphology has been grouped and re-coloured according to the three dominant landform suites indicative of an active temperate glacial landsystem.  
85x191mm (300 x 300 DPI)

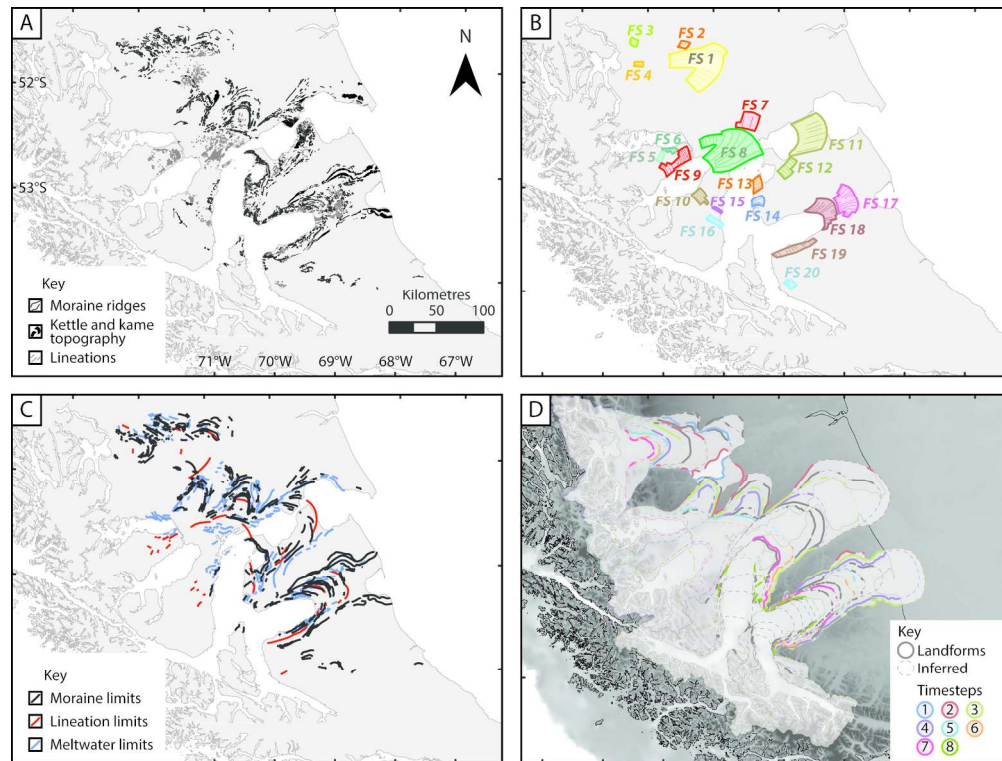


Figure 12. (A) Simplified version of the glacial geomorphology in the study area to show the dominant ice flow and ice marginal features. (B) The flow-sets defined in this study (FS 1-20). (C) The dominant limits associated with four different sets of ice-marginal features. These were synthesised into glacial limits, shown in (D). The two innermost limits of the Skyring lobe are from Kilian et al. (2007). Eight of these limits are used in our glacial reconstruction time steps, coloured according to Figure 14.

183x139mm (300 x 300 DPI)

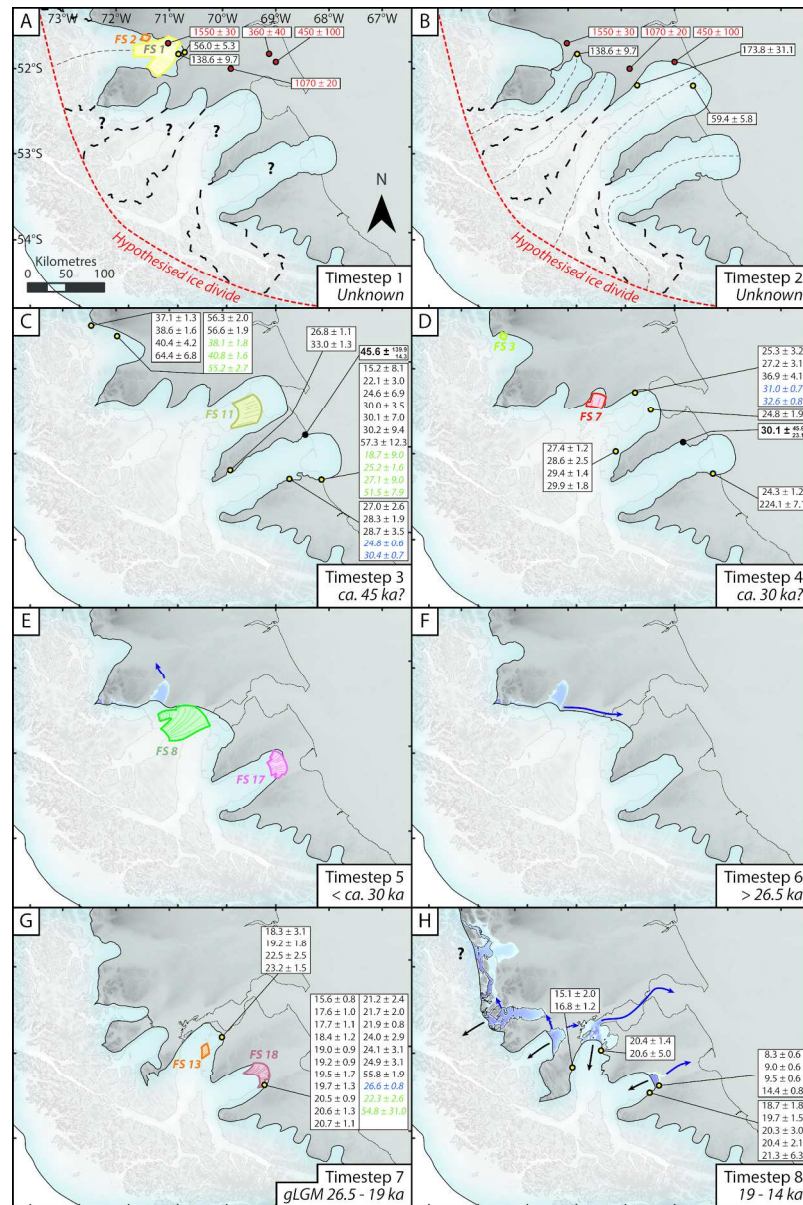


Figure 13. Reconstructed glacial history for the five ice lobes studied, with eight time steps shown in (A) to (H). The hypothesized ice divide based on Hulton et al. (2002) is shown in (A) and (B) for reference. We show the rest of the ice sheet for completeness, with hypothesized gLGM limits based on Coronato et al. (2004). The rest of the ice sheet would have retreated over time, but that was not part of our study. Also shown in (A) and (B) are hypothesized drainage divides between the five ice lobes (bold dashed black lines) and the lines of topographic profiles for each ice lobe shown in Figure 14 (fine dashed black lines). Key flow-sets are shown and blue arrows show the direction of lake drainage routes. Question marks show where the ice configuration is unknown and black arrows in (H) show final retreat during time step 8. Published chronological data are shown where appropriate (see text for discussion). These are: argon dates (red text/circles); cosmogenic nuclide exposure dates (yellow circles) consisting of recalibrated  $^{10}\text{Be}$  dates (black text), recalibrated  $^{26}\text{Al}$  dates (italic blue text) and  $^{36}\text{Cl}$  dates (italic green text); and cosmogenic nuclide depth profiles (bold black text/circles).

163x245mm (300 x 300 DPI)

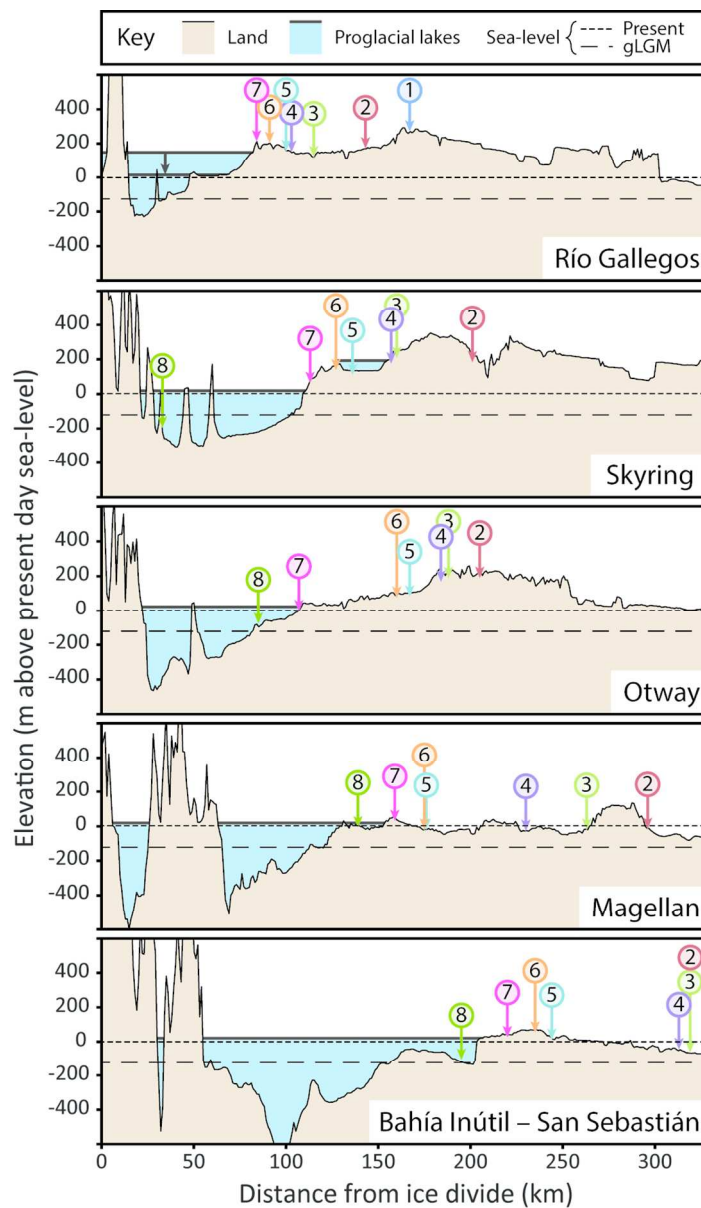


Figure 14. Topographic profiles for each ice lobe, shown as changes in elevation relating to present-day sea-level against distance from the hypothesised ice sheet divide. Ice flowed from left to right. The profiles from the ice divide to the outermost time step are shown in Figure 13A and B. The coloured numbers relate to the time steps shown in Figure 13D. Present-day sea-level is shown (short dashes), as well as the approximate sea-level at the gLGM (long dashes). Hence, the outermost limits of the BI-SSb lobe were in the Atlantic Ocean but would have formed on the exposed continental shelf. Also shown are the approximate heights of former proglacial lakes. The Río Gallegos lake would have dropped progressively over time, but the timing is not well constrained.

87x149mm (300 x 300 DPI)

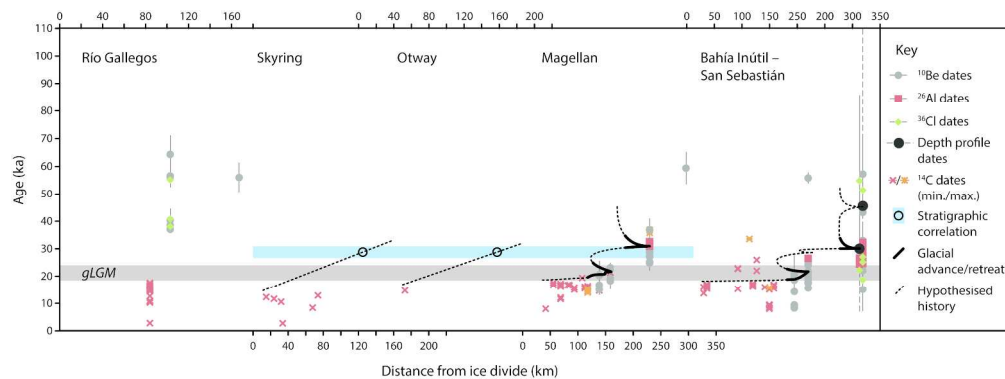


Figure 15. A distance-time graph for the five ice lobes over the last glacial cycle, based on cosmogenic nuclide and radiocarbon dating discussed in the text. Dated lava flows suggest that most of the ice lobes would have advanced during earlier glacial cycles (Meglioli, 1992; Singer et al., 2004; Kaplan et al., 2007). The BI-SSb lobe contains a large number of dates, but with scattered ages and large associated errors. It is not possible to reconcile the cosmogenic nuclide ages and some of the radiocarbon dates during deglaciation. The Magellan lobe contains fewer dates, but a more consistent ice-retreat history. The Otway and Skyring lobes contain few dates, but must have been retreating from a limit prior to ca. 30 ka because of the lake drainage from palaeo-Laguna Blanca in front of the Skyring, Otway and Magellan lobes (the blue stratigraphic correlation bar). Note the similarities in the glacial histories of these four ice lobes, including retreating from extensive positions prior to 30 ka and the gLGM, and rapid late-stage retreat. The timing of advance and retreat of the Río Gallegos lobe is not well constrained, partly because many of the cosmogenic nuclide and radiocarbon dates are from lateral positions that cannot be robustly linked to the former ice terminus. A large number of radiocarbon dates are shown from (Sagredo et al., 2011), but these cannot be tied to the ice terminus and are simply shown against the approximate ice distance in time step 7.

241x89mm (300 x 300 DPI)

## Supplementary Information

### Darvill et al. 'Dynamics of former ice lobes of the southernmost Patagonian Ice Sheet based on a glacial landsystems approach'

---

#### Contents

1	Age recalculation .....	2
1.1	<sup>10</sup> Be and <sup>26</sup> Al exposure ages .....	2
1.2	<sup>36</sup> Cl exposure ages .....	3
1.3	Depth profile exposure ages .....	3
1.4	Radiocarbon ages.....	4
2	Additional chronological discussion.....	9
2.1	Time step 1: Pre-global Last Glacial Maximum (gLGM) advance .....	9
2.2	Time step 2: Pre-gLGM advance .....	9
2.3	Time step 3: Pre-gLGM advance .....	10
2.4	Time step 4: Pre-gLGM advance .....	11
2.5	Time step 5: Re-advances, rapid flow and lake drainage .....	12
2.6	Time step 6: Re-advances, rapid flow and lake drainage .....	12
2.7	Time step 7: The gLGM .....	13
2.8	Time step 8: Rapid retreat.....	13
3	Supplementary references .....	14

#### List of data tables

Table S1.	Compilation of <sup>10</sup> Be and <sup>26</sup> Al cosmogenic nuclide exposure ages from the study area. Ages have been recalculated. ....	5
Table S2.	Compilation of <sup>36</sup> Cl cosmogenic nuclide exposure ages from the study area. Ages have not been recalculated. ....	6
Table S3.	Ages from two depth profiles through outwash associated with glacial limits in the study area. Ages are taken directly from Darvill et al. (2015b).....	6
Table S4.	Compilation of radiocarbon dates relating to glacier activity within the study area. Ages have been recalculated. ....	7

---

## 1 Age recalculation

In order to apply a broad chronological framework to the geomorphological reconstruction in this study, a large number of cosmogenic nuclide exposure ages and radiocarbon ages were compiled (Tables S1, S2, S3 and S4). The  $^{10}\text{Be}$ ,  $^{26}\text{Al}$  and radiocarbon dates were also recalculated. There is an argument that recalculation may not be necessary because:

1. Uncertainty associated with cosmogenic nuclide exposure ages appears to be dominated by post-depositional effects (Kaplan et al., 2007; Evenson et al., 2009; Darvill et al., 2015a, 2015b) rather than uncertainties associated with age calculation.
2. Many of the landforms that have been exposure dated are older than the landforms used for regional or global  $^{10}\text{Be}$  production rate calibrations (these are generally <20 ka; Borchers et al., 2016).

We recalculated ages because many of the original studies were published prior to updated calibration studies (both for cosmogenic nuclide exposure dating and radiocarbon dating). Moreover, whilst many of the ages may be older than the production rate datasets, this is still likely to be a better approximation of age than if older calibration datasets were used, and also creates consistency within our compilation, such that ages are compared on a similar scale. Overall, younger ages within the compilation (e.g. since the global Last Glacial Maximum) are changed little by this recalculation.

### 1.1 $^{10}\text{Be}$ and $^{26}\text{Al}$ exposure ages

A total of 75  $^{10}\text{Be}$  exposure ages and 13  $^{26}\text{Al}$  exposure ages were compiled for this study, shown in Table S1 (McCulloch et al., 2005b; Kaplan et al., 2007, 2008; Evenson et al., 2009; Darvill et al., 2015b; Sagredo et al., 2011). All exposure ages were recalculated using the CRONUS-earth online calculator version 2.2 (Wrapper script: 2.2; Main calculator: 2.1; Objective function: 2; Constants: 2.2.1; Muons: 1.1 (available at <http://hess.ess.washington.edu/math/>; see Balco et al., 2008). All calibration information was

1  
2  
3 taken from the original studies, and a density of  $2.7 \text{ g cm}^{-3}$  was assumed where no density  
4 information was provided (reasonable given that all other published sample densities from  
5 the study area were either  $2.65 \text{ g cm}^{-3}$  or  $2.7 \text{ g cm}^{-3}$ ). No erosion correction was applied so  
6 that the studies could be directly compared in a simple way, although in reality this is almost  
7 certainly unrealistic (Kaplan et al., 2007). The Macaulay River production rate from New  
8 Zealand was used (Putnam et al., 2010) because it overlaps at  $1\sigma$  with a production rate  
9 from Lago Argentino in Patagonia (Kaplan et al., 2011) and has been used in other recent  
10 dating studies in Patagonia (Boex et al., 2013; Darvill et al., 2015b). The choice between  
11 these two production rates does not affect our discussion - the important point is that both  
12 production rates are lower than the global rate used in most of the original studies. Likewise,  
13 we consistently applied the 'Lm' time-dependent scaling scheme of Lal (1991) and Stone  
14 (2000), although the choice of scaling scheme makes little difference within the context of  
15 our discussion.  
16  
17  
18  
19  
20  
21  
22  
23  
24  
25  
26  
27  
28  
29

### 30 **1.2 $^{36}\text{Cl}$ exposure ages**

31  
32 The details of nine  $^{36}\text{Cl}$  exposure ages are compiled in Table S2 (Kaplan et al., 2007;  
33 Evenson et al., 2009). The dates were not recalculated given that progress in determining  
34 local  $^{36}\text{Cl}$  production rates has not been made on the same scale as  $^{10}\text{Be}$  production (and,  
35 by ratio scaling,  $^{26}\text{Al}$  production). All ages were considered underestimates in the original  
36 studies due to postdepositional erosion and/or exhumation.  
37  
38  
39  
40  
41  
42

### 43 **1.3 Depth profile exposure ages**

44  
45 Two exposure ages from depth profiles through outwash sediments related to glacial limits  
46 are compiled in Table S3, with all data from Darvill et al. (2015). These dates are modelled  
47 from numerous depth samples, and the reader is referred to the original study for full details  
48 of the modelling process and contextual discussion.  
49  
50  
51  
52  
53  
54  
55  
56  
57  
58  
59  
60

#### 1.4 Radiocarbon ages

1  
2  
3  
4  
5  
6  
7  
8  
9  
10  
11  
12  
13  
14  
15  
16  
17  
18  
19  
20  
21  
22  
23  
24  
25  
26  
27  
28  
29  
30  
31  
32  
33  
34  
35  
36  
37  
38  
39  
40  
41  
42  
43  
44  
45  
46  
47  
48  
49  
50  
51  
52  
53  
54  
55  
56  
57  
58  
59  
60

Data associated with 114 radiocarbon ages from the study area are compiled in Table S4 (Heusser et al., 1990; Clapperton et al., 1995; Anderson & Archer, 1999; Hall et al., 2013; McCulloch et al., 2005b, 2005a; McCulloch & Bentley, 1998; Uribe, 1982; Heusser, 1987; Porter, 1990; Stern, 1992; McCulloch & Davies, 2001; Kilian et al., 2013; Sagredo et al., 2011). Where the raw  $^{14}\text{C}$  ages and errors were available, dates were re-calibrated with CALIB 7.0 (Stuiver et al., 2005) using the INTCAL13 curve (Reimer, 2013). All dates were sorted according to their context as either minimum (MIN) or maximum (MAX) ages for glacier advances, or bracketed (M/M) where they dated material underlain and overlain by glacial sediments.

Page	2.1	2.7	1	0	170000	20100	S555	1109800	9400	KNSTD	Yes	Boulder	28695	3473	30396	712
2.4	2.7	1	0	167000	10300	S555	904100	9000	KNSTD	Yes	Boulder	28256	1858	24762	593	
1	2.5	2.7	1	0	109000	12200	S555	0	0	KNSTD		Boulder	21223	2432		
2	2.5	2.7	1	0	90400	4650	NIST_30600	0	0	KNSTD		Boulder	17597	985		
3	1.4	2.7	1	0	107000	5430	NIST_30600	849400	18500	KNSTD		Boulder	20662	1144	26583	824
4	1	2.7	1	0	100000	4270	NIST_30600	0	0	KNSTD		Boulder	19020	913		
5	0.5	2.7	1	0	219739	7456	S555	0	0	KNSTD		Boulder	33039	1338		
6	0.5	2.7	1	0	177837	5957	S555	0	0	KNSTD		Boulder	26762	1072		
7	0.9	2.7	1	0	125930	10467	S555	0	0	KNSTD		Boulder	19520	1684		
8	0.6	2.7	1	0	107975	31430	S555	0	0	KNSTD		Boulder	21346	6264		
9	2.9	2.7	1	0	92397	8565	S555	0	0	KNSTD		Boulder	18670	1785		
10	2	2.65	1	0	101010	6427	KNSTD	0	0	KNSTD		Boulder	18401	1241		
11	2	2.65	1	0	112971	6525	KNSTD	0	0	KNSTD		Boulder	20590	1275		
12	2	2.65	1	0	98689	5883	KNSTD	0	0	KNSTD		Boulder	17717	1128		
13	2	2.65	1	0	106896	4586	KNSTD	0	0	KNSTD		Boulder	19197	925		
14	1	2.65	1	0	123064	3493	KNSTD	0	0	KNSTD		Boulder	21938	785		
15	4	2.65	1	0	303471	7871	KNSTD	0	0	KNSTD		Boulder	55846	1907		
16	2	2.65	1	0	111186	4324	KNSTD	0	0	KNSTD		Boulder	20462	914		
17	6	2.65	1	0	82817	4082	KNSTD	0	0	KNSTD		Boulder	15638	844		
18	5	2.65	1	0	104681	6420	KNSTD	0	0	KNSTD		Boulder	19725	1288		
19	3	2.65	1	0	42024	2657	KNSTD	0	0	KNSTD		Boulder	8327	557		
20	3	2.65	1	0	47831	2825	KNSTD	0	0	KNSTD		Boulder	9480	597		
21	2	2.65	1	0	45843	3122	KNSTD	0	0	KNSTD		Boulder	9013	645		
22	2	2.65	1	0	72529	3798	KNSTD	0	0	KNSTD		Boulder	14350	815		
23	6	2.7	0.999999	0	130107	3377	NIST_27900	918950	33591	Z92-0222		Outwash	31022	1053	32404	1396
24	6	2.7	0.999999	0	180591	4619	NIST_27900	868057	29274	Z92-0222	Yes	Outwash	43215	1459	30580	1241
25	6	2.7	0.999999	0	99630	2922	NIST_27900	784025	27306	Z92-0222		Outwash	23704	867	27575	1144
26	6	2.7	0.999999	0	112414	3101	NIST_27900	806137	29141	Z92-0222		Outwash	26770	942	28365	1210
27	6	2.7	0.999999	0	127390	3653	NIST_27900	856986	29261	Z92-0222		Outwash	26633	961	26470	1082
28	6	2.7	0.999999	0	118438	4222	NIST_27900	792773	35652	Z92-0222		Outwash	24750	1036	24463	1234
29	6	2.7	0.999999	0	131073	5696	NIST_27900	819874	26226	Z92-0222		Outwash	27408	1338	25309	987
30	6	2.7	0.999999	0	118430	4081	NIST_27900	860572	36911	Z92-0222		Outwash	24749	1011	26582	1292
31	4	2.7	1	0	148976	8492	S555	0	0	KNSTD		Boulder	29898	1835		
32	4	2.7	1	0	145383	12358	S555	0	0	KNSTD		Boulder	28647	2530		
33	4	2.7	1	0	135386	4874	S555	0	0	KNSTD		Boulder	27394	1156		
34	1.5	2.7	1	0	930000	158000	S555	0	0	KNSTD		Boulder	173758	31085		
35	2.6	2.7	1	0	127000	9490	S555	0	0	KNSTD	Yes	Boulder	24818	1942		
36	1	2.7	1	0	286000	26900	S555	0	0	KNSTD	Yes	Boulder	59402	5817		
37	0.5	2.7	1	0	130000	16200	S555	0	0	KNSTD	Yes	Boulder	25275	3216		
38	1.5	2.7	1	0	143000	16100	S555	1004400	6800	KNSTD	Yes	Boulder	27162	3135	30958	708
39	0.9	2.7	1	0	189000	20600	S555	1032900	9600	KNSTD	Yes	Boulder	36878	4135	32647	776

Table S2. Compilation of  $^{36}\text{Cl}$  cosmogenic nuclide exposure ages from the study area. Ages have not been recalculated.

Author	Year	Glacial system	Moraine system	Time step	Sample name	Latitude (DD)	Longitude (DD)	Outliers?	Sample type	Cl-36 age (years)	Cl-36 error (years)
Kaplan	2007	Bahía Inútil	Rio Cullen	3	RC-04-01	-53.47	-68.321	Yes	Boulder	51500	7900
Kaplan	2007	Bahía Inútil	Rio Cullen	3	RC-04-04f	-53.504	-68.155	Yes	Boulder	25200	1600
Kaplan	2007	Bahía Inútil	B limit	4	TF-04-04	-53.607	-69.233	Yes	Boulder	54800	31000
Kaplan	2007	Bahía Inútil	B limit	4	TF-04-05	-53.605	-69.282	Yes	Boulder	22300	2600
Evenson	2009	Bahía Inútil	Rio Cullen	3	ARG-00-Tdf-039	-	-	Yes	Boulder	18700	9000
Evenson	2009	Bahía Inútil	Rio Cullen	3	ARG-00-Tdf-043	-	-	Yes	Boulder	27100	9000
Evenson	2009	Rio Gallegos	Bella Vista	3	CRG-T32-99-23	-51.69	-72	Yes	Boulder	55200	2700
Evenson	2009	Rio Gallegos	Bella Vista	3	CRG-T41-99-25	-51.69	-72	Yes	Boulder	40800	1600
Evenson	2009	Rio Gallegos	Bella Vista	3	CRG-T41-99-26	-51.69	-72	Yes	Boulder	38100	1800

Table S3. Ages from two depth profiles through outwash associated with glacial limits in the study area. Ages are taken directly from Darvill et al. (2015b).

Author	Year	Glacial system	Moraine system	Time step	Sample name	Latitude (DD)	Longitude (DD)	Outliers?	Sample type	Depth profile age (years)	Depth profile positive error (years)	Depth profile negative error (years)
Darvill	2015b	Bahía Inútil	Rio Cullen outwash	3	Cullen profile	-52.8899	-68.4244		Depth profile	45600	139900	14300
Darvill	2015b	Bahía Inútil	San Sebastian outwash	4	Filaret profile	-52.9743	-68.831		Depth profile	30100	45600	23100

Validation of radiocarbon dates relating to glacier activity within the study area. Ages have been recalculated.

Year	Glacial system	Site	Time step	Sample name	Latitude (DD)	Longitude (DD)	14C date	$\pm 1\sigma$	Calib age	Calib error
1										
2										
3										
4										
5	Bahía Inútil	Chorillo Rosario	8	QL-1683	-53.4476	-70.0901	13280	80	15974	247
6	Bahía Inútil	Chorillo Rosario	8	QL-4293	-53.4476	-70.0901	12010	80	13868	235
7	Bahía Inútil	Chorillo Rosario	8	QL-4294	-53.4476	-70.0901	12060	80	13932	187
8	Bahía Inútil	Punta Cameron	8	A-6791	-53.6871	-69.9249	13030	260	15556	850
9	Bahía Inútil	Puente Charlie	8	A-7569	-53.4294	-70.053	12740	120	15156	485
10	Bahía Inútil	Puente Charlie	8	A-7570	-53.4294	-70.053	7240	70	8063	122
11	Bahía Inútil	Isla Dawson East	4	AA-10414	-53.6333	-70.4667	29500	380	33609	775
12	Bahía Inútil	V17-70	8	CAMS-22179	-53.5667	-70.3	21740	120	25989	226
13	Bahía Inútil	V17-83	8	CAMS-22180	-53.8667	-70.3667	19050	90	22950	330
14	Bahía Inútil	V17-83	8	OS-2164	-53.8667	-70.3667	12850	60	15362	226
15	Bahía Inútil	V17-83	8	OS-2165	-53.8667	-70.3667	18900	80	22757	244
16	Bahía Inútil	V17-70	8	OS-2166	-53.5667	-70.3	18150	100	22024	294
17	Bahía Inútil	Punta Marinelli Bog	8	OS-61545	-54.3412	-69.5313	14050	70	17084	290
18	Bahía Inútil	Punta Marinelli Bog	8	OS-61550	-54.3412	-69.5313	12950	60	15490	235
19	Bahía Inútil	Punta Esperanza	8	OS-61551	-54.3119	-69.949	13350	65	16049	216
20	Bahía Inútil	Punta Marinelli Bog	8	OS-61606	-54.3412	-69.5313	13400	85	16108	272
21	Bahía Inútil	Punta Marinelli Bog	8	OS-63929	-54.3412	-69.5313	13250	55	15927	197
22	Bahía Inútil	Punta Marinelli Bog	8	OS-64068	-54.3412	-69.5313	13250	85	15937	264
23	Bahía Inútil	Punta Marinelli Bog	8	OS-64070	-54.3412	-69.5313	13650	90	16496	313
24	Bahía Inútil	Punta Marinelli Bog	8	OS-64095	-54.3412	-69.5313	13950	55	16896	250
25	Bahía Inútil	Punta Esperanza	8	OS-64245	-54.3119	-69.949	11900	190	13778	468
26	Bahía Inútil	Puente Charlie	8	AA-35087	-53.4294	-70.053	8320	65	9303	173
27	Bahía Inútil	Estancia Cameron II	8	AA-42413	-53.6366	-69.6492	13980	120	16968	412
28	Bahía Inútil	Estancia California	8	AA-42414	-53.5957	-69.5605	13614	86	16445	300
29	Bahía Inútil	Puente Charlie	8	Beta-117945	-53.4294	-70.053	8230	70	9214	192
30	Bahía Inútil	Puente Charlie	8	SRR-6286	-53.4294	-70.053	8545	45	9514	47
31	Bahía Inútil	Puente Charlie	8	SRR-6287	-53.4294	-70.053	10875	45	12755	61
32	Bahía Inútil	Puente Charlie	8	SRR-6288	-53.4294	-70.053	13160	45	15824	191
33	Bahía Inútil	Puente Charlie	8	SRR-6496	-53.4294	-70.053	13205	55	15877	197
34	Bahía Inútil	Puente Charlie	8	SRR-6497	-53.4294	-70.053	12960	55	15500	226
35	Bahía Inútil	Puente Charlie	8	SRR-6498	-53.4294	-70.053	13125	55	15762	240
36	Bahía Inútil	Puente Charlie	8	SRR-6499	-53.4294	-70.053	10830	50	12738	61
37	Bahía Inútil	Puente Charlie	8	SRR-6500	-53.4294	-70.053	7660	50	8465	83
38	Bahía Inútil/Magellan	Estancia Esmerelda II	8	A-6793	-53.584	-70.5041	14260	350	17284	929
39	Bahía Inútil/Magellan	Estancia Esmerelda I	8	A-6807	-53.5917	-70.4648	13425	310	16185	915
40	Bahía Inútil/Magellan	Estancia Esmerelda II	8	A-6814	-53.584	-70.5041	13650	310	16556	895
41	Bahía Inútil/Magellan	Estancia Esmerelda II	8	SSR-5143	-53.584	-70.5041	13890	50	16812	233
42	Cordillera Darwin	Caleta Olla 2	-	OS-61542	-54.9377	-69.1722	10300	50	12111	275
43	Cordillera Darwin	BL-07-15	-	OS-61603	-54.8176	-69.735	9310	65	10486.5	195.5
44	Cordillera Darwin	Ventisquero Holanda 1	-	OS-61638	-54.9441	-69.1317	12550	60	14785.5	355.5
45	Cordillera Darwin	BL-07-16B	-	OS-64237	-54.8235	-69.7364	12350	120	14508.5	492.5
46	Magellan	Pampa Alegre	8	DIC-2322	-53.0709	-70.8725	11940	110	13813	268
47	Magellan	Puerto del Hambre	8	AA-30651	-53.6177	-70.9519	14455	115	17617	317
48	Magellan	Punta Arenas	8	QL-1470	-53.1383	-70.8973	13400	140	16140	415
49	Magellan	Parque Chacabunco	7	QL-1650	-52.95	-70.8333	47000	>	Out of range	-
50	Magellan	Cabo Porpesse	3	QL-1660	-52.95	-70.7833	42400	2500/3700	Out of range	-
51	Magellan	Pampa Alegre	8	np	-53.0709	-70.8725	11795	365	13994	1006

1995	Magellan	Rio Tres Brazos	4	AA-10412	-53.2667	-70.9167	43945	2100	Out of range	-
1995	Magellan	Rio Tres Brazos	4	AA-10413	-53.2667	-70.9167	43810	2120	Out of range	-
1995	Magellan	Estancia Amarillo	8	AA-12872	-53.4036	-70.9863	13945	105	16895	378
1995	Magellan	Rio Tres Brazos	4	AA12875	-53.2667	-70.9167	41900	1700	Out of range	-
1995	Magellan	Rio Tres Brazos	4	AA12875	-53.2667	-70.9167	27690	335	31770	736
1995	Magellan	Rio Tres Brazos	4	AA-8396	-53.2667	-70.9167	47200	>	Out of range	-
1895	Magellan	Pampa Alegre	8	SRR-4583	-53.0709	-70.8725	12070	45	13920	150
1998	Magellan	Cabo Valentin II	8	A-8164	-53.5686	-70.5311	10055	65	11619	328
1998	Magellan	14C Age estimate for Reclus tephra layer	8	AA-20570	-53.6177	-70.9519	12840	100	15377	331
2001	Magellan	Puerto del Hambre	8	CAMS-65903	-53.6177	-70.9519	14470	50	17659	198
2005b	Magellan	Rio Tres Brazos	4	AA-30863	-53.2667	-70.9167	40800	1300	Out of range	-
2005b	Magellan	Rio Tres Brazos	4	AA-30864	-53.2667	-70.9167	41100	1500	Out of range	-
2005b	Magellan	Porvenir 2 kettle hole within terrace	8	AA-30913	-53.3	-70.3333	16090	100	19403	288
2005b	Magellan	14C Age estimate for Reclus tephra layer	8	AA-30918	-53.1383	-70.8973	12525	75	14713	407
2005b	Magellan	Porvenir 2 kettle hole within terrace	7	Beta-117944	-53.3	-70.3333	16130	60	19448	200
2005a	Magellan	Pampa Alegre	8	A-6818	-53.0709	-70.8725	11805	220/215	13642	83
2005a	Magellan	Cabo Valentin II	8	AA-23077	-53.5686	-70.5311	10314	81	12160	355
2005a	Magellan	Bahia Lomas	8	AA-30917	-53.7928	-70.6725	7250	55	8072	102
2005a	Magellan	Punta Arenas	8	AA-30919	-53.1383	-70.8973	13050	95	15620	325
2005a	Magellan	San Felipe	8	AA-35082	-53.6042	-70.9641	13850	90	16753	323
2005a	Magellan	Estancia Guairabo	8	AA-42415	-53.3111	-70.9476	13186	78	15842	268
2005a	Magellan	Estancia Amarillo	8	AA-42416	-53.4036	-70.9863	13849	81	16753	302
2005a	Magellan	Pampa Alegre	8	Beta-117943	-53.0709	-70.8725	12820	100	15342	348
2005a	Magellan	Pampa Alegre	8	SRR-6501	-53.0709	-70.8725	12720	55	15125	210
2005a	Magellan	Pampa Alegre	8	SRR-6502	-53.0709	-70.8725	13155	60	15808	231
2005a	Magellan	Pampa Alegre	8	SSR-6502	-53.0709	-70.8725	13155	60	15808	231
2011	Otway	OTW2	8	-	-52.9663	-72.0214	-	-	14780	-
2011	Rio Gallegos	Eberhardt	7	CAMS 107008	-51.5779	-72.6684	13745	50	16611.5	252.5
2011	Rio Gallegos	Eberhardt	7	CAMS 107052	-51.5779	-72.6684	10695	40	12647.5	69.5
2011	Rio Gallegos	Lago Dorotea	7	CAMS 107053	-51.5336	-72.4829	12670	45	15045.5	213.5
2011	Rio Gallegos	Lago Dorotea	7	CAMS 107054	-51.5336	-72.4829	12460	90	14625.5	434.5
2011	Rio Gallegos	Lago Dorotea	7	CAMS 107055	-51.5336	-72.4829	13000	60	15542	241
2011	Rio Gallegos	Lago Dorotea	7	CAMS 107092	-51.5336	-72.4829	14170	45	17264.5	192.5
2011	Rio Gallegos	Vega Benitez	7	CAMS 107093	-51.5582	-72.5828	14520	140	17674	355
2011	Rio Gallegos	Lago Dorotea	7	CAMS 114975	-51.5336	-72.4829	14105	45	17178.5	212.5
2011	Rio Gallegos	Vega Benitez	7	CAMS 115804	-51.5582	-72.5828	12580	35	14921.5	209.5
2011	Rio Gallegos	Pantano Dumestre	7	CAMS 125918	-51.8053	-72.4356	12910	25	15425.5	171.5
2011	Rio Gallegos	Pantano Laurita	7	CAMS 128971	-51.6788	-72.2741	9570	40	10919	182
2011	Rio Gallegos	Pantano Laurita	7	CAMS 128972	-51.6788	-72.2741	2720	35	2817	62
2011	Rio Gallegos	Pantano Laurita	7	CAMS 128973	-51.6788	-72.2741	9495	35	10836.5	232.5
2011	Rio Gallegos	Lago Arauco	7	CAMS 128974	-51.9663	-72.0434	13330	70	16027.5	226.5
2011	Rio Gallegos	Lago Arauco	7	CAMS 128975	-51.9663	-72.0434	13245	50	15921	186
2011	Rio Gallegos	Lago Arauco	7	CAMS 128976	-51.9663	-72.0434	12500	60	14686	385
2011	Rio Gallegos	Lago Pintito	7	CAMS 128980	-52.0445	-72.3808	13670	50	16501.5	236.5
2011	Rio Gallegos	Lago Pintito	7	CAMS 128981	-52.0445	-72.3808	13610	50	16417.5	212.5
2011	Rio Gallegos	Pantano Dumestre	7	CAMS 129005	-51.8053	-72.4356	12875	45	15387	202
2011	Rio Gallegos	Pantano Dumestre	7	CAMS 129006	-51.8053	-72.4356	12895	45	15410.5	204.5
2011	Rio Gallegos	Eberhardt	7	CAMS 98831	-51.5779	-72.6684	13690	45	16534.5	233.5
2011	Rio Gallegos	Pantano A. Varas	7	CAMS 98832	-51.7589	-72.8112	9210	40	10374	122
2011	Rio Gallegos	Vega Benitez	7	CAMS 98916	-51.5582	-72.5828	12490	40	14678.5	352.5
2011	Rio Gallegos	Vega Benitez	7	CAMS 98917	-51.5582	-72.5828	12225	40	14254	323

## 2 Additional chronological discussion

The relationship between our reconstructed time steps and published chronological constraints is described in Section 6.2 of the main text. However, there are subtleties associated with much of this chronological information that benefit from a more detailed version of this discussion. In this section, we describe the dates available for each ice lobe during each of our reconstructed time steps, and provide the landform context from our reconstruction. It is worth noting that while the dates are from the published literature, we (re-)assign those dates to our eight time steps in this study.

### 2.1 Time step 1: Pre-global Last Glacial Maximum (gLGM) advance

The Río Gallegos lobe flowed rapidly to its greatest extent during time step 1, creating flowsets FS 1 and FS 2 (Figure 13A in the main text). The extent of the other ice lobes is unclear, but the Skyring lobe cannot have been fully extended because the geomorphology of the Río Gallegos and Skyring lobes overlaps and Skyring drainage later flowed into the former Río Gallegos depression. Cosmogenic  $^{10}\text{Be}$  exposure ages of 56.0 ka and 138 ka from the outer limits of the Río Gallegos lobe are substantially younger than the Bella Vista flow, which has been  $^{40}\text{Ar}/^{39}\text{Ar}$  dated to 1.17 Ma (Kaplan et al., 2007; Singer et al., 2004; Meglioli, 1992). The Bella Vista flow underlies till deposits thought to relate to the maximum glacial advance and the large difference in these ages may be due to post-depositional processes affecting moraine boulders sampled for exposure dating (Kaplan et al., 2007). We caution that linking distal drift sediments to limits defined by glacial geomorphology is challenging (e.g. Meglioli (1992) also dated flows to 8.0 and 8.5 Ma within this ice lobe); the Bella Vista flow only provides a maximum age for the limit; and it is not inconceivable that the ice lobe extended towards this maximum extent on several occasions.

### 2.2 Time step 2: Pre-gLGM advance

The Skyring, Otway, Magellan and BI-SSb ice lobes advanced to their maximum extents, whereas the Río Gallegos lobe retreated (Figure 13B in the main text). The Skyring lobe

1  
2  
3 advanced into the Río Gallegos depression, overriding former moraines and glacial  
4 lineations to leave irregular dissected ridges (Section 4.2.3 in the main text). The precise  
5 extent and timing of the advances is unclear, and correlation cannot be made between the  
6 ice lobes. The  $^{10}\text{Be}$  ages of 56.0 ka and 138 ka (Kaplan et al., 2007) in time step 1 could  
7 reasonably relate to time step 2 if they were actually deposited by the Skyring lobe. Two  
8 additional  $^{10}\text{Be}$  ages of 59.4 ka and 173 ka from the Magellan lobe are similarly young  
9 compared to local  $^{40}\text{Ar}/^{39}\text{Ar}$  ages (Meglioli, 1992; Singer et al., 2004; Kaplan et al., 2007).  
10 However, tying dated tills to glacial limits may not be straightforward. It is conceivable that  
11 the ice lobes advanced more than once to similar limits at radically different times, possibly  
12 due to topographic constraints (Kirkbride & Winkler, 2012; Barr & Lovell, 2014) or erosional  
13 feedbacks (Kaplan et al., 2009; Anderson et al., 2012). For example, The BI-SSb lobe was  
14 also close to this limit in at least time steps 3 and 4. The four cosmogenic dates available for  
15 time steps 1 and 2 may indicate two separate advances at around 173-138 ka and 59-56 ka,  
16 but the dates are not apparently in stratigraphic order. These dates also disagree with the  
17 conceptual age model for the region (Meglioli, 1992) and do not take into account erosion  
18 and/or exhumation processes (Kaplan et al., 2007).  
19  
20  
21  
22  
23  
24  
25  
26  
27  
28  
29  
30  
31  
32  
33  
34  
35

### 36 **2.3 Time step 3: Pre-gLGM advance**

37  
38 The Río Gallegos lobe continued to recede during time step 3 and the Skyring and Otway  
39 lobes retreated to close to the limits of their topographic basins (Figure 13C in the main text).  
40 The Magellan lobe may have re-advanced to form FS 11, although this flowset could equally  
41 have formed in time step 1 or 2. In the Río Gallegos lobe, two  $^{10}\text{Be}$  ages of 56.3 ka and 56.6  
42 ka and three  $^{36}\text{Cl}$  ages of 38.1 ka to 55.2 ka are younger than expected (repeat samples;  
43 Evenson et al., 2009). However, four  $^{10}\text{Be}$  ages of between 37.1 ka and 64.4 ka from interior  
44 lateral moraines may have been deposited at a similar time (Sagredo et al., 2011). There are  
45 no chronological constraints for the Skyring, Otway or Magellan lobes and correlation  
46 between the lobes cannot be made. The BI-SSb ice limit has been  $^{10}\text{Be}$  dated (Kaplan et al.,  
47 2007, 2008), with twelve ages ranging from 15.2 ka to 57.3 ka, eight of which are within 26.8  
48  
49  
50  
51  
52  
53  
54  
55  
56  
57  
58  
59  
60

1  
2  
3 ka and 33.0 ka. In addition, two  $^{26}\text{Al}$  dates of 24.8 ka and 30.4 ka and four  $^{36}\text{Cl}$  dates of 18.7  
4 ka, 25.2 ka, 27.1 ka and 51.5 ka have been reported (Kaplan et al., 2007; Evenson et al.,  
5 2009). Post-depositional erosion and exhumation may have affected many of these boulder  
6 ages (Kaplan et al., 2007), so Darvill et al. (2015b) used a  $^{10}\text{Be}/^{26}\text{Al}$  depth profile through  
7 outwash sediments to obtain an independent estimate of age for the BI-SSb lobe. This  
8 demonstrated that the limit was deposited during the last glacial cycle, possibly around 45.6  
9 ka.  
10  
11

12  
13  
14  
15  
16  
17  
18 Numerous dating campaigns have yielded ages younger than previously thought, and a best  
19 estimate of age for time step 3 may be somewhere between 26.8 ka and 57.3 ka. The large  
20 spread of ages could result from post-depositional processes, possibly linked to gradual  
21 melt-out of the dead ice in hummocky terrain or boulder erosion (Kaplan et al., 2007;  
22 Schomacker, 2008; Darvill et al., 2015a). The latter could explain the offset between the  
23 dominant cluster of boulder ages between 27.0 ka and 36.2 ka, and the depth profile at 45.6  
24 ka, in which case the depth profile would be a better estimate of the time of deposition.  
25  
26  
27  
28  
29  
30  
31

#### 32 33 **2.4 Time step 4: Pre-gLGM advance**

  
34

35  
36 In time step 4, the Skyring and Otway lobes retreated to skirt the edges of their respective  
37 basins, with the Otway lobe possibly re-advancing to form FS 7 (Figure 13D in the main  
38 text). The Magellan lobe retreated to Primera Angostura and the Río Gallegos lobe  
39 continued to retreat, possibly re-advancing slightly to deposit FS 3. The BI-SSb lobe re-  
40 advanced close to the limit of time step 3, yielding two  $^{10}\text{Be}$  dates of 24.3 ka and 224.1 ka  
41 (Kaplan et al., 2007). These dates are ambiguous, but a depth-profile through associated  
42 outwash yielded a more robust age of ca. 30.1 ka (Darvill et al., 2015b). Like time step 3,  
43 there is scatter in the boulder ages, perhaps due to post-depositional processes. For the  
44 Magellan lobe, four  $^{10}\text{Be}$  ages between 24.8 ka and 36.9 ka and two  $^{26}\text{Al}$  ages of 31.0 ka and  
45 32.6 ka (Kaplan et al., 2007) imply that the limit may have been deposited at a similar time to  
46 that of the BI-SSb lobe. In addition, we suggest that four  $^{10}\text{Be}$  dates of 27.4 ka to 29.9 ka on  
47  
48  
49  
50  
51  
52  
53  
54  
55  
56  
57  
58  
59  
60

1  
2  
3 Kaplan et al., 2008), may have been deposited at this time given the similarity in ages. There  
4 are no ages for the Río Gallegos, Skyring or Otway lobes and it remains unclear to what  
5 extent these lobes acted in a similar manner.  
6  
7

### 8 9 10 **2.5 Time step 5: Re-advances, rapid flow and lake drainage**

11  
12 The Río Gallegos, Magellan and Skyring lobes retreated during time step 5, with the latter  
13 triggering the development of a proglacial lake – palaeo-Laguna Blanca – which may have  
14 further facilitated ice loss from a calving front (Figure 13E in the main text). This lake drained  
15 northwards into the Río Gallegos depression, indicating recession of the Río Gallegos lobe.  
16  
17 The Otway lobe re-advanced significantly, forming FS 8 around Laguna Cabeza del Mar and  
18 shifting the ice divide between the Otway and Magellan lobes south-eastward into the  
19 present-day Strait of Magellan. The BI-SSb lobe also re-advanced to a limit close to Bahía  
20 San Sebastián, depositing a large terminal moraine that is still preserved east of Laguna  
21 Larga and forming FS 17. The re-advances of these two ice lobes may have been in  
22 response to rapid ice flow, or possible surge-like activity. Thus, between time steps 4 and 5,  
23 all ice lobes receded and the Otway and BI-SSb lobes re-advanced. There are no  
24 chronological constraints for any of the ice lobes in this time step, but the moraines  
25 deposited by the Otway can be correlated with those of the Skyring and Magellan lobes.  
26  
27  
28  
29  
30  
31  
32  
33  
34  
35  
36  
37  
38

### 39 40 **2.6 Time step 6: Re-advances, rapid flow and lake drainage**

41  
42 All ice lobes retreated during this time step (Figure 13F in the main text). The Skyring, Otway  
43 and Magellan lobes did not retreat far because the potentially catastrophic drainage of  
44 palaeo-Laguna Blanca passed from in front of the Skyring lobe east to south-easterly in front  
45 of the Otway and Magellan lobes. It is unclear how far the Río Gallegos and BI-SSb lobes  
46 retreated during this time step, but the presence of deformed lacustrine sediments in re-  
47 advance moraines of the BI-SSb lobe in time step 7 suggests that this ice lobe must have  
48 retreated sufficiently for a pro-glacial lake to develop. Again, there are no chronological  
49 constraints for any of the ice lobes in this time step, but we note that for the Skyring, Otway  
50  
51  
52  
53  
54  
55  
56  
57  
58  
59  
60

1  
2  
3 and Magellan lobes, time steps 5 and 6 are broadly constrained by dates in the Magellan  
4 lobe for time steps 4 and 7, and that the limits can be correlated reasonably robustly across  
5 the three ice lobes. Dating the drainage of palaeo-Laguna Blanca would improve this  
6 chronology and test our interpretation of the dates for time steps 4 and 7.  
7  
8  
9

### 10 11 12 **2.7 Time step 7: The gLGM**

13  
14 This time step has previously been defined as the gLGM limit (Figure 13G in the main text).  
15 There are no supporting ages for the Río Gallegos, Skyring and Otway lobes, although they  
16 were likely situated within the present-day fjords, with the termini of the Skyring and Otway  
17 lobes splitting after time step 6. The Magellan and BI-SSb lobes had retreated – although it  
18 is not clear how far – and re-advanced during this time step, possibly displaying surge-like  
19 behaviour and forming FS 13 and FS 18. The Magellan lobe has been  $^{10}\text{Be}$  dated four times  
20 on Península Juan Mazía to between 18.3 ka and 23.2 ka. The BI-SSb lobe has also been  
21 dated with 18  $^{10}\text{Be}$  dates yielding ages of between 15.6 ka and 55.8 ka, one  $^{26}\text{Al}$  date of 26.6  
22 ka, and two  $^{36}\text{Cl}$  dates of 22.3 ka and 54.8 ka (McCulloch et al., 2005b; Kaplan et al., 2007,  
23 2008; Evenson et al., 2009). Sixteen of the  $^{10}\text{Be}$  dates fall between 17.6 ka and 24.9 ka.  
24 The reason for the scatter in ages is unclear, although the  $^{10}\text{Be}$  date of 55.8 ka may be due  
25 to inheritance, given most of the dates are from a large erratic boulder train on the south-  
26 eastern side of Bahía Inútil (Darvill et al., 2015a). Nonetheless, the dates for the Magellan  
27 and BI-SSb lobes generally support the assertion that this time step relates to the gLGM.  
28  
29  
30  
31  
32  
33  
34  
35  
36  
37  
38  
39  
40  
41  
42

### 43 44 **2.8 Time step 8: Rapid retreat**

45  
46 All of the ice lobes were in full post-gLGM retreat during this time-step, likely developing  
47 proglacial lakes in front of their receding margins that could have increased the rate of ice  
48 retreat due to frontal calving (Figure 13H in the main text; Porter et al., 1992; Kilian et al.,  
49 2007). The Skyring and Otway lobes were located well within their respective fjords, with  
50 cores suggesting ice-free conditions in Seno Skyring and Seno Otway dated to at least 14.8  
51 ka and 14.7 ka, respectively, using radiocarbon dating and tephrostratigraphy (Kilian et al.,  
52  
53  
54  
55  
56  
57  
58  
59  
60

1  
2  
3 2013). Kilian et al. (2007) suggested that this was part of a rapid retreat of the Skyring lobe,  
4 likely linked in part to proglacial calving. The Magellan lobe has been  $^{10}\text{Be}$  dated to 20.4 ka  
5 and 20.6 ka on Península Juan Mazía and also 15.1 ka and 16.8 ka on the western lateral  
6 side of the lobe (Kaplan et al., 2008), perhaps indicating relatively rapid retreat of the ice  
7 lobe during and after this time step, and supporting ice recession by ca. 22 ka, as indicated  
8 by luminescence ages on the western side of the Strait of Magellan (Blomdin et al., 2012).  
9 The BI-SSb lobe has yielded five similar  $^{10}\text{Be}$  dates between 18.7 ka and 21.3 ka (McCulloch  
10 et al., 2005b; Kaplan et al., 2008), as well as four  $^{10}\text{Be}$  dates from below the proglacial lake  
11 shoreline suggesting that drainage may have occurred between 14.4 ka and 8.3 ka  
12 (Evenson et al., 2009). Numerous radiocarbon dates suggest that retreat of the Magellan  
13 and BI-SSb ice lobes was well under way by at least 14-15 ka (Clapperton et al., 1995;  
14 McCulloch & Bentley, 1998; McCulloch et al., 2005b), although the presence of the Reclús  
15 tephra within lake sediments suggests full retreat and lake drainage cannot have been  
16 before ca. 14.3 ka (McCulloch et al., 2005a). The rapid retreat, and possible collapse, of the  
17 BI-SSb lobe during and after this time step is supported by radiocarbon dates in the  
18 accumulation area of the lobe in central Cordillera Darwin that suggest that the constituent  
19 outlet glaciers that formed the ice lobe in this time step may have retreated into small interior  
20 fjords as early as 16.8 ka (Hall et al., 2013).  
21  
22  
23  
24  
25  
26  
27  
28  
29  
30  
31  
32  
33  
34  
35  
36  
37  
38  
39  
40  
41  
42

### 43 **3 Supplementary references**

44  
45  
46 Anderson, D.M. & Archer, R.B. (1999). Preliminary evidence of early deglaciation in southern  
47 Chile. *Palaeogeography Palaeoclimatology Palaeoecology* **146** (1-4), 295–301.

48  
49  
50  
51 Anderson, R.S., Dühnforth, M., Colgan, W. & Anderson, L. (2012). Far-flung moraines:  
52 Exploring the feedback of glacial erosion on the evolution of glacier length.  
53 *Geomorphology* **179**, 269–285.  
54  
55  
56

57  
58 Balco, G., Stone, J.O., Lifton, N.A. & Dunai, T.J. (2008). A complete and easily accessible  
59  
60

1  
2  
3 means of calculating surface exposure ages or erosion rates from  $^{10}\text{Be}$  and  $^{26}\text{Al}$   
4 measurements. *Quaternary Geochronology* **3** (3), 174–195.  
5  
6

7  
8 Barr, I.D. & Lovell, H. (2014). A review of topographic controls on moraine distribution.  
9  
10 *Geomorphology* **226**, 44–64.  
11

12  
13 Blomdin, R., Murray, A., Thomsen, K.J., Buylaert, J.-P., Sohbati, R., Jansson, K.N. &  
14  
15 Alexanderson, H. (2012). Timing of the deglaciation in southern Patagonia: Testing the  
16  
17 applicability of K-Feldspar IRSL. *Quaternary Geochronology* **10** (0), 264–272.  
18

19  
20 Boex, J., Fogwill, C., Harrison, S., Glasser, N.F., Hein, A., Schnabel, C. & Xu, S. (2013).  
21  
22 Rapid thinning of the late Pleistocene Patagonian Ice Sheet followed migration of the  
23  
24 Southern Westerlies. *Sci. Rep.* **3**, 1–6.  
25

26  
27 Borchers, B., Marrero, S., Balco, G., Caffee, M., Goehring, B., Lifton, N., Nishiizumi, K.,  
28  
29 Phillips, F., Schaefer, J. & Stone, J. (2016). Geological calibration of spallation  
30  
31 production rates in the CRONUS-Earth project. *Quaternary Geochronology* **31**, 188–  
32  
33 198.  
34

35  
36 Clapperton, C.M., Sugden, D.E., Kaufman, D.S. & McCulloch, R.D. (1995). The Last  
37  
38 Glaciation in Central Magellan Strait, southernmost Chile. *Quaternary Research* **44** (2),  
39  
40 133–148.  
41

42  
43 Darvill, C.M., Bentley, M.J. & Stokes, C.R. (2015a). Geomorphology and weathering  
44  
45 characteristics of erratic boulder trains on Tierra del Fuego, southernmost South  
46  
47 America: Implications for dating of glacial deposits. *Geomorphology* **228**, 382–397.  
48

49  
50 Darvill, C.M., Bentley, M.J., Stokes, C.R., Hein, A.S. & Rodés, Á. (2015b). Extensive MIS 3  
51  
52 glaciation in southernmost Patagonia revealed by cosmogenic nuclide dating of  
53  
54 outwash sediments. *Earth and Planetary Science Letters* **429**, 157–169.  
55

56  
57 Evenson, E.B., Burkhart, P.A., Gosse, J.C., Baker, G.S., Jackofsky, D., Meglioli, A., Dalziel,  
58  
59  
60

1  
2  
3 I., Kraus, S., Alley, R.B. & Berti, C. (2009). Enigmatic boulder trains, supraglacial rock  
4 avalanches, and the origin of 'Darwin's boulders,' Tierra del Fuego. *GSA Today* **19** (12),  
5 4–10.  
6  
7

8  
9  
10 Hall, B.L., Porter, C.T., Denton, G.H., Lowell, T. V & Bromley, G.R.M. (2013). Extensive  
11 recession of Cordillera Darwin glaciers in southernmost South America during Heinrich  
12 Stadial 1. *Quaternary Science Reviews* **62** (0), 49–55.  
13  
14

15  
16 Heusser, C.J. (1987). Fire history of Fuego-Patagonia. *Quaternary of South America and*  
17 *Antarctic Peninsula* **5**, 93–109.  
18  
19

20  
21 Heusser, C.J., Heusser, L.E. & Hauser, A. (1990). A 12 000 yr BP Tephra layer at Bahía  
22 Inútil (Tierra del Fuego, Chile). *Anales del Instituto de la Patagonia* **19**, 39–49.  
23  
24

25  
26 Kaplan, M.R., Coronato, A., Hulton, N.R.J., Rabassa, J.O., Kubik, P.W. & Freeman, S.P.H.T.  
27 (2007). Cosmogenic nuclide measurements in southernmost South America and  
28 implications for landscape change. *Geomorphology* **87** (4), 284–301.  
29  
30  
31

32  
33 Kaplan, M.R., Fogwill, C.J., Sugden, D.E., Hulton, N., Kubik, P.W. & Freeman, S.P.H.T.  
34 (2008). Southern Patagonian glacial chronology for the Last Glacial period and  
35 implications for Southern Ocean climate. *Quaternary Science Reviews* **27** (3-4), 284–  
36 294.  
37  
38  
39  
40

41  
42 Kaplan, M.R., Hein, A.S., Hubbard, A. & Lax, S.M. (2009). Can glacial erosion limit the  
43 extent of glaciation? *Geomorphology* **103** (2), 172–179.  
44  
45  
46

47  
48 Kaplan, M.R., Strelin, J.A., Schaefer, J.M., Denton, G.H., Finkel, R.C., Schwartz, R.,  
49 Putnam, A.E., Vandergoes, M.J., Goehring, B.M. & Travis, S.G. (2011). In-situ  
50 cosmogenic  $^{10}\text{Be}$  production rate at Lago Argentino, Patagonia: Implications for late-  
51 glacial climate chronology. *Earth and Planetary Science Letters* **309** (1-2), 21–32.  
52  
53  
54

55  
56 Kilian, R., Baeza, O., Ríos, F., Arz, H., Lamy, F., Witz, J. & Baque, J. (2013). Evolución  
57  
58  
59  
60

1  
2  
3 paleogeográfica y palaeoecológica del Sistema de fiordos del Seno Skyring y Seno  
4 Otway en la región de Magallanes durante el tardiglacial y Holoceno. *Anales del*  
5 *Instituto de la Patagonia*. [Online]. 41 (2) p.5–26.  
6  
7

8  
9  
10 Kilian, R., Schneider, C., Koch, J., Fesq-Martin, M., Biester, H., Casassa, G., Arévalo, M.,  
11 Wendt, G., Baeza, O. & Behrmann, J. (2007). Palaeoecological constraints on late  
12 Glacial and Holocene ice retreat in the Southern Andes (53°S). *Global and Planetary*  
13 *Change* **59** (1–4), 49–66.  
14  
15  
16

17  
18  
19 Kirkbride, M.P. & Winkler, S. (2012). Correlation of Late Quaternary moraines: impact of  
20 climate variability, glacier response, and chronological resolution. *Quaternary Science*  
21 *Reviews* **46** (0), 1–29.  
22  
23  
24

25  
26 Lal, D. (1991). Cosmic ray labeling of erosion surfaces: in situ nuclide production rates and  
27 erosion models. *Earth and Planetary Science Letters* **104** (2–4), 424–439.  
28  
29

30  
31 McCulloch, R.D. & Bentley, M.J. (1998). Late glacial ice advances in the Strait of Magellan,  
32 southern Chile. *Quaternary Science Reviews* **17** (8), 775–787.  
33  
34

35  
36 McCulloch, R.D., Bentley, M.J., Tipping, R.M. & Clapperton, C.M. (2005a). Evidence for late-  
37 glacial ice dammed lakes in the central Strait of Magellan and Bahia Inutil,  
38 southernmost South America. *Geografiska Annaler Series a-Physical Geography* **87A**  
39 (2), 335–362.  
40  
41  
42

43  
44  
45 McCulloch, R.D. & Davies, S.J. (2001). Late-glacial and Holocene palaeoenvironmental  
46 change in the central Strait of Magellan, southern Patagonia. *Palaeogeography*  
47 *Palaeoclimatology Palaeoecology* **173** (3-4), 143–173.  
48  
49

50  
51  
52 McCulloch, R.D., Fogwill, C.J., Sugden, D.E., Bentley, M.J. & Kubik, P.W. (2005b).  
53 Chronology of the last glaciation in central Strait of Magellan and Bahia Inutil,  
54 southernmost South America. *Geografiska Annaler Series a-Physical Geography* **87A**  
55 (2), 289–312.  
56  
57  
58  
59  
60

- 1  
2  
3 Meglioli, A. (1992). *Glacial Geology and Chronology of southernmost Patagonia and Tierra*  
4 *del Fuego, Argentina and Chile*. Lehigh.  
5  
6  
7  
8 Porter, S., Clapperton, C. & Sugden, D. (1992). Chronology and dynamics of deglaciation  
9 along and near the Strait of Magellan, southernmost South America. *SGU series Ca.*  
10 *Research paper*  
11  
12  
13  
14 Porter, S.C. (1990). Character and ages of Pleistocene Drifts in a transect across the Strait  
15 of Magellan. *Quaternary of South America and Antarctica Peninsula* **7**, 35–49.  
16  
17  
18  
19 Putnam, A.E., Schaefer, J.M., Barrell, D.J.A., Vandergoes, M., Denton, G.H., Kaplan, M.R.,  
20 Finkel, R.C., Schwartz, R., Goehring, B.M. & Kelley, S.E. (2010). In situ cosmogenic  
21  $^{10}\text{Be}$  production-rate calibration from the Southern Alps, New Zealand. *Quaternary*  
22 *Geochronology* **5** (4), 392–409.  
23  
24  
25  
26  
27  
28 Reimer, P. (2013). IntCal13 and Marine13 Radiocarbon Age Calibration Curves 0–50,000  
29 Years cal BP. *Radiocarbon* **55** (4), 1869–1887.  
30  
31  
32  
33 Sagredo, E.A., Moreno, P.I., Villa-Martinez, R., Kaplan, M.R., Kubik, P.W. & Stern, C.R.  
34 (2011). Fluctuations of the Última Esperanza ice lobe (52°S), Chilean Patagonia, during  
35 the last glacial maximum and termination 1. *Geomorphology* **125** (1), 92–108.  
36  
37  
38  
39 Schomacker, A. (2008). What controls dead-ice melting under different climate conditions? A  
40 discussion. *Earth-Science Reviews* **90** (3–4), 103–113.  
41  
42  
43  
44 Singer, B.S., Ackert, R.P. & Guillou, H. (2004).  $^{40}\text{Ar}/^{39}\text{Ar}$  and K-Ar chronology of  
45 Pleistocene glaciations in Patagonia. *Geological Society of America Bulletin* **116** (3-4),  
46 434–450.  
47  
48  
49  
50  
51  
52 Stern, C.R. (1992). Tefrocronología de Magallanes: nuevos datos e implicaciones. *Anales*  
53 *del Instituto de la Patagonia* **21**, 129–141.  
54  
55  
56  
57 Stone, J.O. (2000). Air pressure and cosmogenic isotope production. *J. Geophys. Res.* **105**  
58  
59  
60

1  
2  
3 (B10), 23753–23759.  
4

5  
6 Stuiver, M., Reimer, P.J. & Reimer, R.W. (2005). *CALIB 5.0*. 2005.  
7  
8 <http://calib.qub.ac.uk/calib/>.  
9

10  
11 Uribe, P. (1982). Deglaciación en el sector central del Estrecho de Magallanes:  
12 consideraciones geomorfológicas y cronológica. *Anales del Instituto de la Patagonia*  
13 **13**, 103–111.  
14  
15  
16  
17  
18  
19  
20  
21  
22  
23  
24  
25  
26  
27  
28  
29  
30  
31  
32  
33  
34  
35  
36  
37  
38  
39  
40  
41  
42  
43  
44  
45  
46  
47  
48  
49  
50  
51  
52  
53  
54  
55  
56  
57  
58  
59  
60